Frontiers in Scientific Research and Technology

Online ISSN: 2682-2970
Print ISSN: 2682-2962
http://fsrt.journals.ekb.eg

FSRT J 12 (2025) 56 – 80 10.21608/fsrt.2025.413874.1174

Geochemical and Mineralogical Investigation of Gabbros and Surrounding Granitic Rocks in Abu Murrat Area, Eastern Desert, Egypt: A Review in Petrogenesis of Gabbros Bearing Fe-Ti oxide Ores

Doaa Ashraf Abdelnaiem[a,*], S. Kharbish[a], A. Abdelnasser[b,c], A. El-Awady[d]

[a]Geology Department, Faculty of Science, Suez University, Suez, Egypt.

[b]Geological Engineering Department, Faculty of Mines, Istanbul Technical University, Istanbul 34469, Turkey.

[c]Geology Department, Faculty of Science, Benha University, 13518 Benha, Egypt.

[d]Geology Department, Faculty of Science, Zagazig University, Zagazig 44519, Egypt.

ARTICLE INFO

Article history:
Submitted 13 August 2025
Received in revised form 24 September 2025
Accepted 28 September 2025
Available online1 October 2025

Keywords
Arabian–Nubian Shield;
I-type and A-type granites;
arc-related magmatism;
post-collisional setting;
gabbroic intrusions;
Fe–Ti–P oxide ores;
liquid immiscibility;
continental rifting;
magmatic differentiation;
AFC processes;
tectonomagmatic evolution.

ABSTRACT

This article reviews previous works and integrates them with newly generated datasets to reconstruct the petrogenetic evolution of the Abu Murrat intrusions in Egypt's Northern Eastern Desert. The Wadi Baroud area hosts a diverse suite of Neoproterozoic igneous rocks, including older granites (I-type), younger gabbros, and younger granites (A-type) alongside a range of associated mineralizations including Fe-Ti-P oxide ores and rare metals. These lithologies form part of the northern Arabian–Nubian Shield and record the magmatic and tectonic evolution during the late stages of the Pan-African orogeny. The results highlight a three-stage magmatic evolution: (1) early arc-related granitoids formed by hydrous mantle melting, (2) layered gabbros crystallized from tholeiitic melts with strong fractional crystallization and crustal contamination, and (3) younger granites derived from partial melting of metasedimentary crust during post-collisional extension, Geochemical modeling (Rayleigh and AFC) further demonstrates the transition from mantle-derived tholeiitic magmas to crustally contaminated derivatives. The review concludes that the Abu Murrat complex offers an example of linked mantle- and crust-derived magmatism, illustrating the shift from subduction-related processes to extensional tectonics during the Neoproterozoic Era. The review also represents data about the nature and origin of associated mineralization, including Fe–Ti–P oxide mineralization and rare metals.

1. Introduction

1.1. Geological background of Arabian Nubian Shield

The Arabian–Nubian Shield (ANS) constitutes a major component of Egypt's Neoproterozoic basement and represents the northern segment of the East African Orogen (EAO) (Stern, 1994), a vast orogenic system that evolved over roughly 300 million years. The ANS is largely composed of juvenile crust formed between 900 and 550 Ma (Johnson et al., 2011; Fritz et al., 2013: Sami et al., 2022, 2023). Its geological history records a succession of tectono-magmatic processes, beginning with oceanic arc volcanism (900–700 Ma), followed by the accretion of arc terranes (800–650 Ma), and culminating in the collision of East and West Gondwana. Subsequent lithospheric thinning and extensional tectonics occurred between 630 and 550 Ma.

* Corresponding author at Suez University

E-mail addresses: doaaashraf036@gmail.com (Doaa Ashraf Abdelnaiem)

Researchers generally divide the ANS evolution into three main tectonic stages: pre-collisional (800–750 Ma), syn-collisional (720–630 Ma), and post-collisional (620–580 Ma) (Stern, 1994, 2002, 2008; Hargrove et al., 2006; Vaughan and Pankhurst, 2008; Avigad and Gvirtzman, 2009; Stern and Johnson, 2010; Johnson et al., 2011; Be'eri-Shlevin et al., 2012; Ali et al., 2013; Fritz et al., 2013). The post-collisional stage is characterized by extensive crustal melting, resulting in the emplacement of both calc-alkaline and alkaline intrusions (Fritz et al., 2013; Hamimi et al., 2021; Adam et al., 2022; Abdelfadil et al., 2013).

Situated within the ANS, Egypt's Eastern Desert is geologically significant due to its wide range of igneous rock types, including I-type granitoids, A-type granites, and layered gabbros, each representing distinct stages of tectonic and magmatic development. The area is well known for its concentration of economically important elements such as niobium, tantalum, rare earths, uranium, thorium, and iron-titanium oxides resources formed through complex magmatic differentiation (El Bialy and Omar, 2015; Khedr et al., 2020, 2022; Frihy, 2007). The

localization of these mineral deposits is largely controlled by regional tectonic structures like the Najd fault system (Khedr et al., 2024). Among the notable sites, Abu Murrat stands out for its low radioactivity Fe-Ti ores, which offer promising potential for safe industrial exploitation. From a research perspective, the Eastern Desert provides an exceptional field setting for investigating mineral formation, crust mantle dynamics, and processes involved in the growth and assembly of continental crust. Our synthesis suggests that the Abu Murrat–Wadi Al-Baroud intrusions represent post-collisional gabbro–granite associations linked to lithospheric extension and mantle–crust interaction within the Northern Eastern Desert. Similar conclusions were reached for other post-collisional mafic–ultramafic intrusions in the Arabian–Nubian Shield, such as the El Bola complex (Abdelfadil et al., 2025), where mantle processes and magma evolution provide a useful comparative framework for interpreting the petrogenesis of the studied gabbros."

1.2 Overview of the Abu Murrat Area

Situated on the northern part of Egypt's Eastern Desert, Wadi Al-Baroud is a segment of the ANS characterized by a wide range of igneous lithologies. The Abu Murrat region is traversed by the Abu Hadieda and Ras Baroud wadis and lies about 25 km SW of Safaga City along the Qena–Safaga Road. It is positioned near the structural boundary separating the Northern and Central Eastern Desert (Stern and Hedge, 1985) and NE of the Um Taghir and Ras Baroud areas. Geographically, it spans longitudes 33°43′40″–33°49′05″ E and latitudes 26°43′52″–26°46′32″ N (Fig. 1). The area is covered by older granites, younger gabbros, younger granites, alongside microgranite offshoots, mafic to felsic dikes, and Fe-Ti oxide ores linked to Neoproterozoic mafic intrusions (El Bialy and Omar,2015; Abed et al., 2021; Awad et al., 2022a; Abuamarah et al., 2023; El-Awady et al., 2025). This region is significant due to its varied igneous rock assemblages, which reflect multiple stages of crustal growth and tectonic activity. The older granites are linked to early arc magmatism and crustal accretion, while the younger granites reflect later crustal melting associated with extensional settings following continental collision (El Bialy and Omar, 2015).

The ANS, one of the largest exposures of juvenile Neoproterozoic continental crust (1000–525 Ma) worldwide (Robinson et al., 2014), hosts Fe–Ti oxide-rich gabbroic intrusions linked to post-collisional magmatism. These intrusions, which occur as both layered and massive bodies, are enriched in titanomagnetite, hemo-ilmenite, and related oxide minerals formed through fractional crystallization and liquid immiscibility processes. Their crystallization took place under conditions of elevated oxygen fugacity at moderate crustal depths, with emplacement guided by the NW–SE-trending Najd fault system. Unlike ores from surrounding localities, those in Abu Murrat display relatively low natural radioactivity, enhancing their suitability for industrial use. The area offers significant insights into mafic intrusion petrogenesis, ore deposition, and the tectono-magmatic evolution of the late Neoproterozoic (Awad et al., 2022a; El-Awady et al., 2025).

1.3 Research Gap and Objectives of This Review

Despite numerous studies focusing on individual Neoproterozoic intrusions in the North Eastern Desert (NED) of Egypt such as Abu Murrat, Wadi Al-Baroud, and Abu Hadieda a comprehensive regional synthesis that integrates the petrological, tectonic, and metallogenic evolution of both mafic and felsic suites remains lacking. Previous work has primarily treated these occurrences in isolation, without fully linking their petrogenesis, geochemical trends, tectonic setting, and ore-forming processes within a unified framework. Moreover, the relationship between post-collisional gabbroic intrusions and their spatially associated I-type and A-type granitoids is still underexplored. The genesis and economic significance of Fe–Ti–P oxide mineralization, particularly in post-collisional settings, also require further clarification in terms of source characteristics, crystallization mechanisms, and structural controls. A detailed regional integration is essential to resolve these gaps and develop a holistic tectono-magmatic model for the NED within the broader Arabian–Nubian Shield (ANS) context.

Research Objectives

1. **To synthesize and compare** the petrological and structural features of Neoproterozoic mafic and felsic intrusions (gabbros, I-type granites, and A-type granites) across key localities in the NED.
2. **To trace** the petrogenetic history of these rock suites through assessment of their magma origins, crystallization conditions, and associated tectonic settings**.**
3. **To investigate the relationship** between post-collisional mafic intrusions and surrounding granitoids, focusing on their associations.
4. **To investigate the genesis of Fe–Ti–P oxide mineralization** in gabbroic intrusions, focusing on magmatic controls including liquid immiscibility, fractional crystallization, and crust–mantle interaction.
5. **To evaluate the structural controls** (e.g., Najd Fault System) influencing intrusion emplacement and ore distribution.
6. **To propose an integrated tectono-magmatic model** linking magmatic evolution, metallogeny, and geodynamic processes in the northern ANS.

2. Regional Framework of the North Eastern Desert

The NED of Egypt, forming part of ANS, comprises a wide spectrum of Neoproterozoic igneous rocks ranging from mafic to felsic compositions. These suites were emplaced during successive tectonomagmatic stages, including arc-related, collisional, and post-collisional magmatism. The assemblages include I-type and A-type granitoids, as well as both massive and layered gabbros. The regional tectonic framework is dominated by NW–SE trending shear zones, most notably the Najd Fault System, which exerted significant control over magma emplacement and acted as a conduit and trap for mineralization (Khedr et al., 2020; El-Bialy and Omar, 2015).

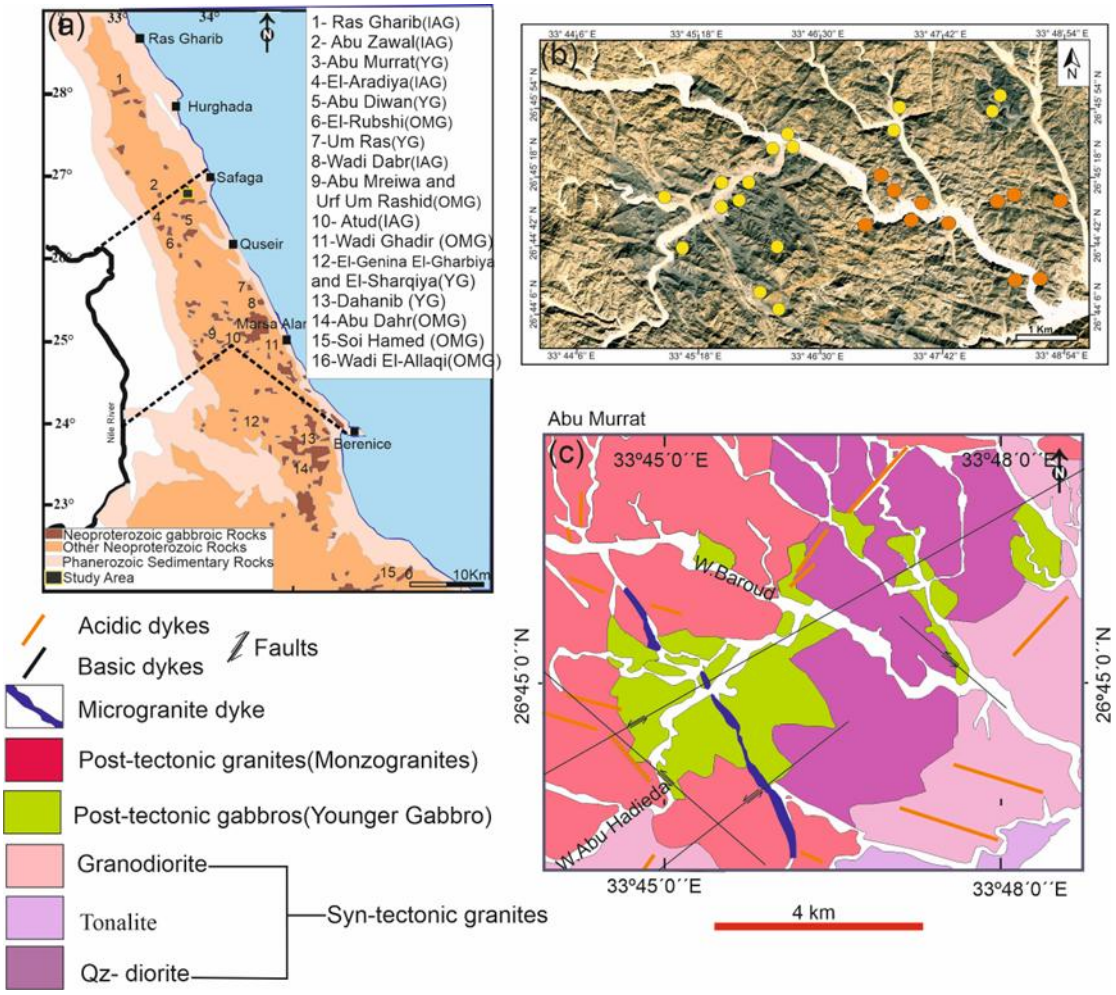

Fig. 1. a) Lithological distribution in Egypt's Eastern Desert, **b)** satellite-based location map, and **c)** geological layout of the Abu Murrat area (modified from Awad et al., 2022a).

2.1. Tectonic Setting

Egypt's NED records a series of Neoproterozoic tectonic stages tied to the East African Orogeny, progressing through early, syn-, and late-collisional events (Ali et al., 2012).

The Older Granite suite, emplaced between ~820 and 615 Ma, constitutes a substantial portion of the ED basement, representing about 27% of its total area (Stern, 1979). Lithologically, these granitoids range from quartz diorite and tonalite to granodiorite (El-Bialy and Omar, 2015) and are chiefly calc-alkaline, I-type rocks. Their genesis is linked to subduction-related continental arc magmatism that was active throughout much of the Neoproterozoic (ca. 850–615 Ma), reflecting long-lived convergence along the ANS margin (Hussein et al., 1982; Stern and Hedge, 1985; Hassan and Hashad, 1990; Stern, 1994; Kröner et al., 1994; Moghazi, 2002; Moussa et al., 2008; El-Mahallawi and Ahmed, 2012).

Multiple magmatic phases have been proposed: the Shaitian (850–800 Ma), Hafafit (760–710 Ma), and Meatiq (630–610 Ma) episodes Hassan and Hashad (1990). Most of these granites crystallized in the pre-collisional phase (850–650 Ma) (Stern, 1994), and show varying levels of deformation. Later intrusions, particularly during the collision phase (650–620 Ma), led to the emplacement of slightly deformed granodioritic bodies (Greiling et al., 1994).

The Younger Granites (610–590 Ma) form about 16% of the Eastern Desert basement and include evolved calc-alkaline I-type and A-type granites (Stern, 1979). Their compositions range from alkali feldspar granites to **s**yenogranites and monzogranites, showing mainly peraluminous to slightly metaluminous characters (Ali et al., 2012).

These granites formed during the post-collisional phase of the ANS. Although some are anorogenic A-type granites, initially classified separately (G3) Hussein et al. (1982), recent data indicates they may have formed contemporaneously with the main Younger Granite suite Eyal et al., 2010).

The post-collisional stage also includes younger gabbroic intrusions that show no signs of metamorphism or deformation, such as the Wadi Abu Hadieda Mafic Intrusion and the El-Baroud layered gabbros. These mafic

bodies are thought to have been derived from a lithospheric mantle source previously altered by subduction-related melts during an earlier phase of Arabian-Nubian Shield development (Abdelfadil et al., 2022; Khedr et al., 2024). Their generation likely resulted from crustal extension and thinning associated with the post-orogenic setting. The El-Baroud gabbros, in particular, are believed to have formed during arc-related rifting, crystallizing at high oxygen fugacity, with temperatures from 800 to 1000 °C and pressures near 3 kbar (Khedr et al., 2024).

The post-collisional gabbros, characterized by their younger, unaltered, and undeformed nature, are located in Egypt's Eastern Desert (Abdelfadil et al., 2022). These intrusions developed during the post-collision stage of the Arabian-Nubian Shield, approximately between 620 and 580 million years ago, following the convergence of the juvenile ANS crust with older continental fragments from pre-Neoproterozoic western Gondwana (Azer et al., 2019). . This stage is marked by crustal thinning and the emergence of alkaline magmatic activity. On tectonic discrimination diagrams, these gabbros commonly reflect within-plate or post-orogenic geodynamic settings (Abdelfadil et al., 2022).

2.2. Structural Controls

The structural framework of the NED is strongly influenced by major strike-slip faults, most notably the Najd Fault System (NW–SE to WNW–ESE), which has guided the development of geological structures and controlled related mineralization. This system exerts significant influence on the alignment of bimodal dikes, foliation patterns in pyroxene gabbros, and the emplacement of Fe–Ti oxide layers and rare-metal-bearing granites, particularly in the El-Baroud area (Khedr et al., 2024). Additional strike-slip systems include NE–SW-trending conjugate faults such as the Qena–Safaga Shear Zone, the largest fault zone in the central Eastern Desert, which separates oceanic from continental arc-related terranes and facilitated the emplacement of diverse magmatic rocks (El-Gaby et al., 1988). In Wadi Al-Baroud, left-lateral WNW–ESE faults caused approximately 1.6 km of horizontal displacement, shifting the northern granodiorites of Gabal Al-Baroud nearly 1 km eastward (Awad et al., 2022b). Smaller NE- or NW-trending strike-slip faults also affect the Abu Hadieda Mafic Intrusion, showing both sinistral and dextral movements (Abdelfadil et al., 2022). Normal faults are pervasive across the mapped lithologies, predominantly oriented NE–SW and WNW–ESE, with less frequent E–W trends (Awad et al., 2022b), while thrust faults formed under NE–SW compression and are accompanied by cataclastic rocks along fault planes, reflecting significant tectonic shortening (Awad et al., 2022b). Dikes are widespread, especially within granitic terrains, trending mainly WNW–ESE and NW–SE with some E–W and N–S orientations. They range from 30 cm to 15 m in thickness and up to 10 km in length, with some tilting attributed to E–W strike-slip activity (Awad et al., 2022b). These dikes vary in composition from basic to acidic types, including basalt, andesite, and granite, and commonly intrude older granitoids and gabbros along NE–SW shear zones, such as in Wadi Abu Hadieda. Many of these microgranite dikes are enriched in rare and radioactive minerals such as zircon, monazite, thorite, uranothorite, allanite, and pyrochlore (Abed et al., 2021), while magmatic veins and dike swarms trending WNW are spatially associated with zones like the Qena–Safaga shear zone (Omran, 2014). Structural fabrics also include NW-trending foliations in older granites and Fe–Ti-rich gabbroic host rocks (Khedr et al., 2024; El-Bialy and Omar, 2021), joint sets in younger granites typically arranged in one or two nearly perpendicular directions (El-Bialy and Omar, 2015), and folding structures such as the Um Taghir syncline in the south, which formed under N–S compression and is characterized by E–W axial planes (Awad et al., 2022b).

3. Geology and Petrography of the Wadi Al-Baroud (Abu Murrat Areas)

The Wadi Al-Baroud area is underlain predominantly by basement rocks consisting mainly of two distinct granite suites: the Older Granites, Younger Gabbros and Younger Granites.

3.1. Older Granite Suite (I-type, Syntectonic)

Generally, The Older Granites, also known as syn-tectonic granitoids, form a widespread batholithic body that stretches across the transitional zone separating the northern and central Eastern Desert. These granitoids cover an estimated 60 km², forming low to moderate topographic features. This suite is largely made up of grayish granodiorite–tonalite rocks, often showing gneissic or massive structures and typically featuring fine mafic inclusions (El Bialy and Omar,2015).

A closer view reveals that older granites in Abu Murrat area span a compositional range from quartz diorite through tonalite to granodiorite. Older granites form moderately elevated, weathered hills with features like fracturing, exfoliation, and spheroidal weathering (Fig. 2a). It includes quartz diorite, tonalite, and granodiorite, intruded by monzogranites (Fig. 2b) and crosscut by dikes and quartz veins (Fig. 2c). Mafic and microdioritic enclaves are common, especially near monzogranite contacts, with some foliation and jointing observed. Petrographically, quartz diorite displays a hypediomorphic texture and is primarily made up of plagioclase, hornblende, quartz, and biotite, with alteration to sericite and chlorite (Fig. 2d). Tonalite is medium-grained, with quartz, plagioclase, and biotite ± hornblende, showing features like pericline twinning and chloritization (Fig. 2e). Granodiorite also shows hypediomorphic texture and consist of feldspars, quartz, biotite, and hornblende, with deformation features and mineral replacements evident (Fig. 2f).

3.2. Younger Granite Suite (A-type, Post-collisional)

In Wadi Al-Baroud, the Younger Granite assemblage is represented by two separate plutons Gabal Ras Baroud and Gabal Abu Hawis (El Bialy and Omar, 2015) which intrude into the Older Granite bodies along distinct, sharp boundaries. These granitic masses form the highest relief in the region.

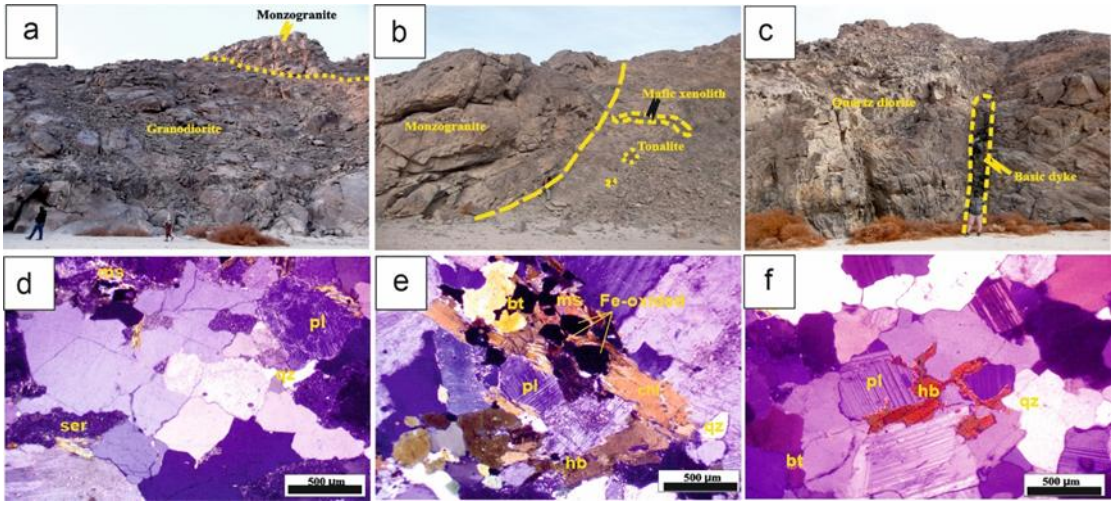

Fig. 2. Field photos showing features of Abu Murrat older granites: (a) Granodiorite intruded by monzogranite; (b) sharp contact between tonalite, including mafic xenoliths and monzogranite; (c) basic dyke intruding quartz-diorite. Under crossed-polarized light, photomicrographs reveal; (d) Sericitized plagioclase and quartz in tonalite; (e) Biotite flakes, hornblende, plagioclase, and Fe-Ti oxides in quartz diorite; (f) Interstitial biotite and quartz between plagioclase in granodiorite.

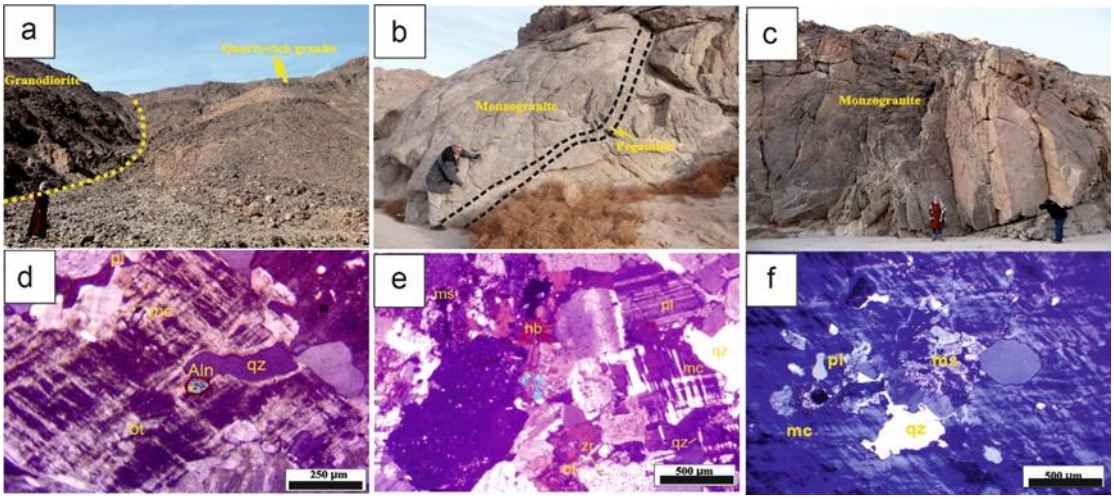

Fig. 3. Field photos illustrating the younger granites of the Abu Murrat area. **(a)** Sharp contact between granodiorite and quartz- rich granite; **(b)** Pegmatite veins traversing monzogranite; **(c**) General feature of jointed monzogranite**.** Photomicrographs photos, all photos were taken under Crossed Nicole; (d) Allanite typically forms short prismatic crystals within microcline in monzogranite. (e) Quartz intergrowth within microcline in monzogranite. (f) Microcline poikilitically enclosing numerous quartz grains in monzogranite.

They are pink to reddish in colour and consist mainly of monzogranites bearing biotite or both biotite and muscovite, typically exhibiting a uniform medium- to coarse-grained texture. Gabal Ras Baroud, nearly circular in outline and covering around 40 km², often contains coarse pegmatitic veins along its margins. The smaller Gabal Abu Hawis pluton, elliptical in form and about 8 km² in area, shows little to no pegmatite development (El Bialy and Omar, 2015). Notably, the muscovite-rich monzogranites in this suite are enriched with Nb-Ta oxide mineralization (Abuamarah et al., 2023).

According to our study, we observe that the younger granites at Abu Murrat form the region's highest and steepest peaks, composed mainly of pink to red monzogranites and quartz-rich granites. These resistant rocks intrude the Older Granites with sharp contacts (Fig. 3a) and sometimes contain quartz diorite xenoliths. Despite their durability, they show weathering features like spheroidal boulders and exfoliation. The granites are cut by quartz and pegmatite veins (Fig. 3b) and display fine-grained chilled margins. Structurally, they are intensely jointed, with prominent E–W and N–S trending joints linked to regional faults (Fig. 3c). Petrographically, monzogranites

are coarse-grained, pink to reddish rocks with an allotriomorphic granular texture, composed of alkali feldspar, plagioclase, quartz, and minor biotite, with accessory phases like zircon and monazite, and alteration minerals such as muscovite and chlorite (Fig. 3d, e). Alkali feldspars display perthitic textures, while quartz shows intergrowth and wavy extinction, enclosing accessory minerals (Fig. 3e). Quartz- rich granites are compositionally similar but contain more quartz beside lesser alkali feldspar and plagioclase (Fig. 3f).

3.3 Gabbroic Intrusions and Their Characteristics

Previous study of Abu Murrat gabbroic intrusion comprises pyroxene-dominated gabbros that intrude older granitic rocks and host notable Fe-Ti oxide mineralization (El Bialy and Omar, 2015; Abdelfadil et al., 2022; Khedr et al., 2024). Gabbros occur in both layered and unlayered forms. Unlayered gabbros are coarse-grained, fresh, and exhibit spheroidal weathering, while layered gabbros are more altered and sometimes host ilmenite-rich layers. Petrographically, the gabbros are classified as pyroxene hornblende gabbro and leucogabbro (Awad et al., 2022a). The Abu Hadieda intrusion primarily consists of pyroxene-hornblende gabbros that intrude older granitoids through distinct contacts (Attawiya et al., 1996). These gabbros are generally dark green, coarse-grained, and undeformed, showing minimal alteration (Abdelfadil et al., 2022).

In the present study, Abu Murrat gabbroic intrusion is characterized by a diverse assemblage of gabbro types, including pyroxene gabbros, pyroxene–hornblende gabbros, hornblende gabbros, biotite–hornblende gabbros, and leucogabbros. Overall, these rocks are largely fresh, though some areas display minor to considerable degrees of alteration. These gabbro shows sharp contacts with surrounding granitoids and features blocky, exfoliated outcrops containing large tonalite–granodiorite xenoliths (Fig. 4a, b), and hosts Fe-Ti-(P) ore as layered oxide bodies in its upper part and less common lenticular lenses in the lower sections (Fig. 4c, d). These rocks exhibit varied grain sizes and cumulate textures, with modal variations in plagioclase, pyroxenes, hornblende, biotite, and apatite, along with abundant Fe-Ti oxides. Fe-Ti oxides mainly magnetite, ilmenite, and titanomagnetite display diverse textures and are closely associated with apatite content (Fig. 5).

3.4 Mineralization Patterns (Fe-Ti Oxide Ores in Gabbros)

Previous work on Abu Murrat (at Wadi Al Baroud) ore bodies mainly titanomagnetite with lesser ilmenite and magnetite occur as veins, layers, and lenses, aligning with the NW-SE Najd fault system. Their emplacement reflects tectonic control and magmatic processes, particularly liquid immiscibility. Compared to the Central and Southern Eastern Desert, El-Baroud is the only known Fe-Ti-rich mafic intrusion in the NED, highlighting its unique geological significance (El Bialy and Omar, 2015).

Abu Murrat Fe–Ti–(P) ores are classified into three types based on Fe–Ti oxide (magnetite, ilmenite) and silicate gangue content: (1) Disseminated ore with up to 20 vol.% Fe-Ti oxides in host gabbros or 25–35 vol.% within ore bands (Fig. 4a–f); (2) Semi-massive ore comprising 50–60 vol.% Fe-Ti oxides (Fig. 4g–i); and (3) Massive ore with 75–85 vol.% oxide content, confined to ore layers and lenses (Fig. 4j–l). Abu Murrat disseminated, semi-massive, and massive Fe–Ti–(P) ores consist mainly of titanomagnetite and ilmenite with variable silicate phases. Apatite is abundant in disseminated ores but absent in denser ores, where Fe-Ti oxides form triple junctions and host pyrite inclusions.

Nb-Ta Oxide Minerals

Numerous mineralogical investigations by Abuamarah et al. (2023) have shown that Wadi Al-Baroud muscovite monzogranite facies hosts columbite, tantalite, and wodginite, Columbite-(Mn) cores are frequently overgrown or partially replaced by tantalite-(Fe) and wodginite, resulting from late-stage interactions with highly fractionated residual melts or fluids. Though our surveys, we concluded that columbite is the main Nb–Ta oxide mineral in Gabel Ras Baroud. It shows a typical zoning pattern, with Nb-rich cores characterized by Ta/(Nb + Ta) values of about 0.11 and Mn/(Mn + Fe) ratios around 0.52, grading outward to mantles enriched in both Ta and Mn, where Ta/(Nb + Ta) can reach 0.31 and Mn/(Mn + Fe) up to 0.79 (Abuamarah et al., 2023). So they classify it as manganocolumbite on the columbite–tantalite diagram (Fig. 7). In contrast to columbite-(Fe) from Mount El-Sibai (neer to the study area), which displays consistently low Ta/(Ta + Nb) (<0.02) and Mn/(Fe + Mn) ratios (0.11–0.19). Such variations highlight late-stage fluid–melt interaction and localized fractionation, pointing to a higher degree of magmatic evolution in Abu Baroud(Sami et al., 2023).

4. Geochemical features

In this section, we rely on data collected from previously published papers For the granitic rocks, we use geochemical data reported by El Bialy and Omar (2015) and Abuamarah et al. (2023), whereas the geochemical data for the younger gabbros are from our own analyses.

4.1. Granitic Rocks

Several geochemical studies have revealed that Older granites are identified as magnesian, metaluminous I-type rocks within the calc-alkaline series (El Mahallawi and Ahmed, 2012). They are marked by elevated strontium levels and a noticeable depletion in elements as Rb, Nb, Y, and REEs. Their geochemical signatures particularly the low Rb/Sr ratio (averaging 0.07) and Nb content below 15 ppm suggest formation in subduction-related arc environments (El Bialy and Omar, 2015). The Younger Granites are high-K, peraluminous A-type rocks, varying from ferroan to magnesian (El Bialy and Omar, 2015; Frost and Frost, 2011; Chappell et al., 2012). They are enriched in Ga, Y, HFSEs (Zr, Hf, Nb, Ta), and REEs (~232 ppm), but show low levels of Ba, Sr, Rb, and transition metals (Bonin, 2007; El Bialy and Omar,2015; Abuamarah et al., 2023). High Rb/Sr and Ga/Al_2O_3 ratios reflect advanced differentiation. Significant negative Eu deviation (Eu/Eu* = 0.10–0.44) indicate low oxygen fugacity, while Ba, Sr, P, and Ti depletion points to fractionation of plagioclase, apatite, and Fe-Ti oxides (Chen et al., 2002; Mansouri et al., 2010; El Bialy and Omar, 2015).

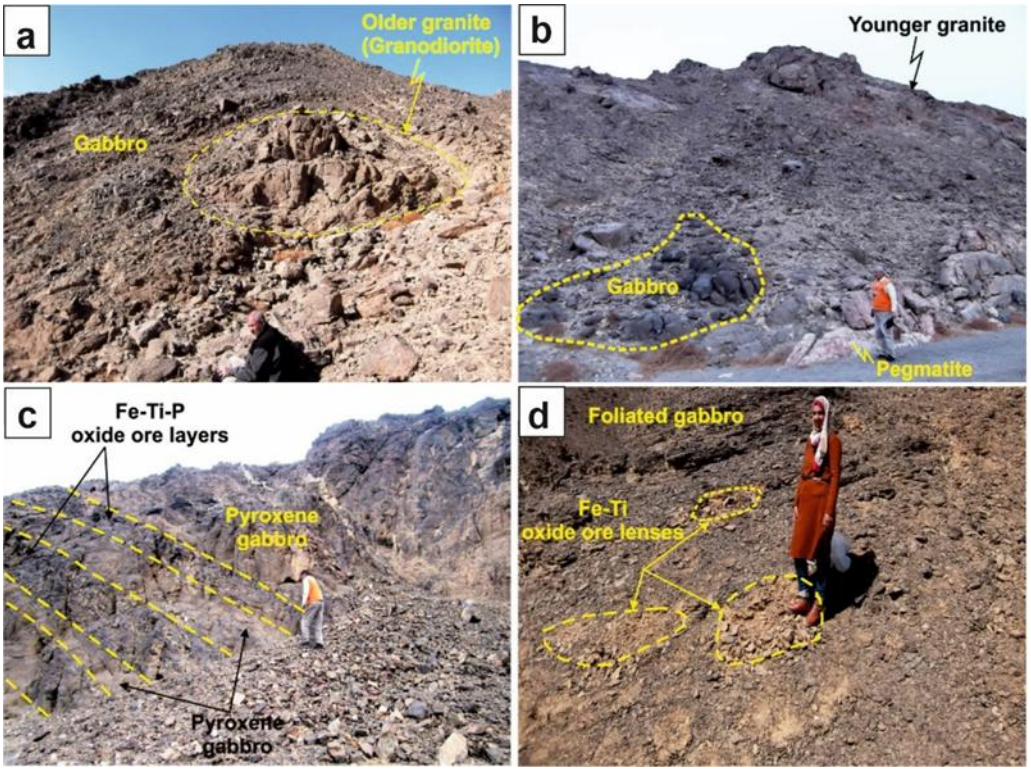

Fig. 4. Field photographs illustrating Abu Murrat gabbroic rocks: (a) Large xenolith of older granite enclosed within younger gabbros; (b) Younger gabbroic blocks occurring as sizable xenoliths in younger granites; (c) Parallel bands or layers of Fe–Ti–P oxide ore hosted in younger gabbros; (d) Small Fe–Ti oxide ore lenses occurring within foliated (sheared) younger gabbros.

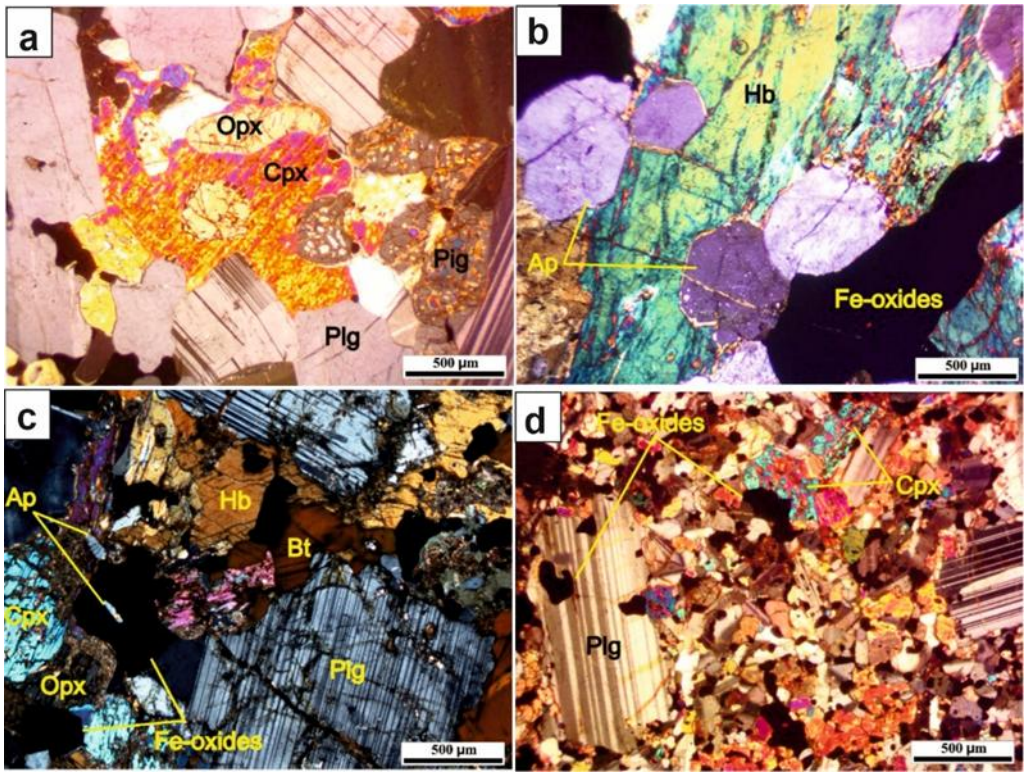

Fig. 5. Photomicrographs of gabbroic rocks under crossed-polarized light: (a) Intercumulus clinopyroxene enclosing orthopyroxene with exsolved blebs of inverted pigeonite in leucogabbros; (b) Large six-sided apatite crystals enclosed within hornblende oikocrysts, forming poikilitic texture alongside intercumulus Fe-oxides in hornblende–pyroxene gabbros; (c) Small cumulus crystals of clinopyroxene, orthopyroxene, and apatite with intercumulus biotite, hornblende, quartz, and Fe–Ti oxides producing a hypediomorphic texture in pyroxene–hornblende gabbros; (d) Plagioclase occurring as large prisms (phenocrysts) and smaller laths intergrown with clinopyroxene and Fe–Ti oxides in the groundmass of fine-grained gabbros.

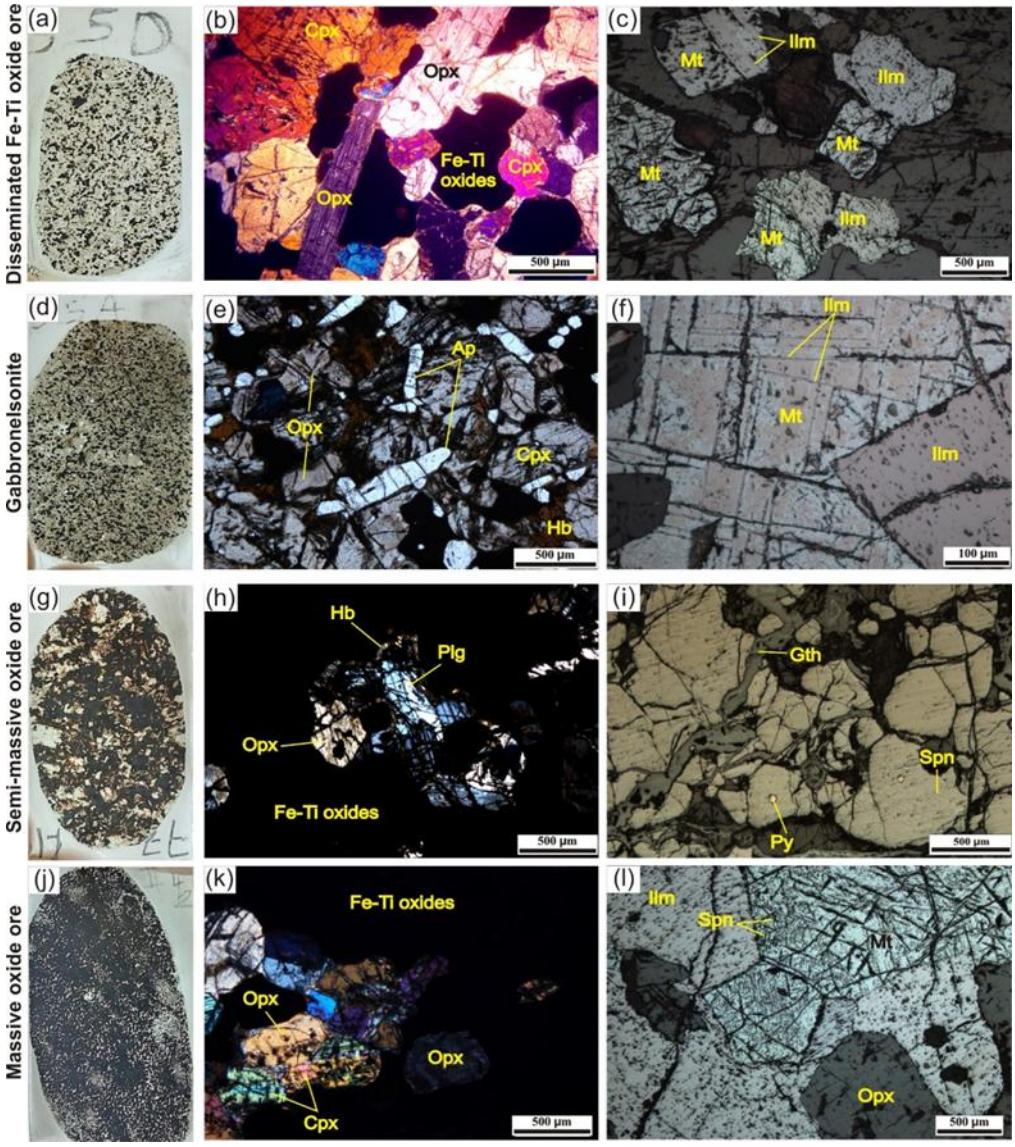

Fig. 6. Thin section photographs and photomicrographs of Abu Murrat Fe–Ti–(P) oxide ores: (a, d, g, j) Thin sections photos showing different types of Fe-Ti-(P) oxide ores. (b, h, k) Photomicrographs taken under crossed polarized light. (e) Photomicrograph taken under plane polarized light. (c, f, i, l) Photomicrographs taken under reflected light. (a) Disseminated ore; (b) Intercumulus Fe–Ti oxides filling spaces between Opx and Cpx, disseminated ore; (c) Magnetite–ilmenite composite grain with banded intergrowth; (d) Disseminated Fe–Ti–(P) ore in gabbro-nelsonite; (e) Cumulus apatite with prismatic/six-sided sections surrounded by Opx, Cpx, hornblende, and Fe–Ti oxides, gabbro-nelsonite; (f) Ilmenite–magnetite contact, magnetite martitized with ilmenite lamellae, gabbro-nelsonite; (g) Semi-massive ore; (h) Plagioclase and Opx corroded by and enclosing Fe–Ti oxides rimmed by hornblende, semi-massive ore; (i) Magnetite with pyrite inclusions, spinel exsolution lamellae, and goethite alteration, semi-massive ore; (j) Massive ore; (k) Cumulus Opx and Cpx corroded by Fe–Ti oxides, massive ore; (l) Ilmenite–magnetite contact with triple junctions and magnetite-hosted spinel lamellae, massive ore.

The Abu Murrat Older Granite suite closely matches the geochemical features of Wadi Al-Baroud granitoids (El Bialy and Omar, 2015; Abuamarah et al., 2023), showing a metaluminous, calc-alkaline composition (Fig. 8c) and moderate evolution, with LREE enrichment over HREE and minor negative Eu anomalies (Fig. 9). By contrast, the Younger Granite suite is highly siliceous, metaluminous to peraluminous, ferroan (Fig. 8b, c), and exhibits strong LREE enrichment relative to HREE with pronounced negative Eu anomalies (Fig. 9).

4.2. Gabbroic Rocks

Khedr et al. (2024) studied Al-Baroud gabbroic rocks and stated that they are classified as pyroxene gabbros and gabbronorites with variable SiO_2 (34.0-53.33wt%) and high Al_2O_3 (9.92-18wt%), Sr (395-768ppm), Fe_2O_3 (8.8-16.5wt%), TiO_2 (0.9-7.19wt%), and P_2O_5 (>2.48wt%) contents. A strong correlation between Al_2O_3 and Sr indicates plagioclase as the major Sr-bearing phase (Prowatke and Klemme, 2006).

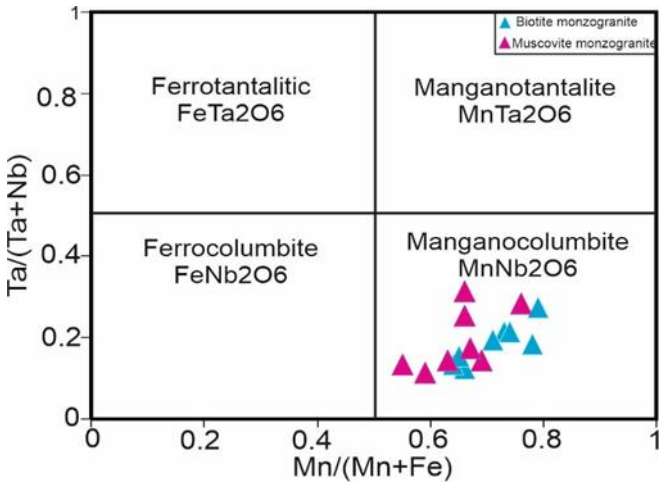

Fig. 7. Columbite–tantalite quadrilateral diagram illustrating the chemical classification of columbite-group minerals Černý (1989), these data are from Abuamarah et al. (2023).

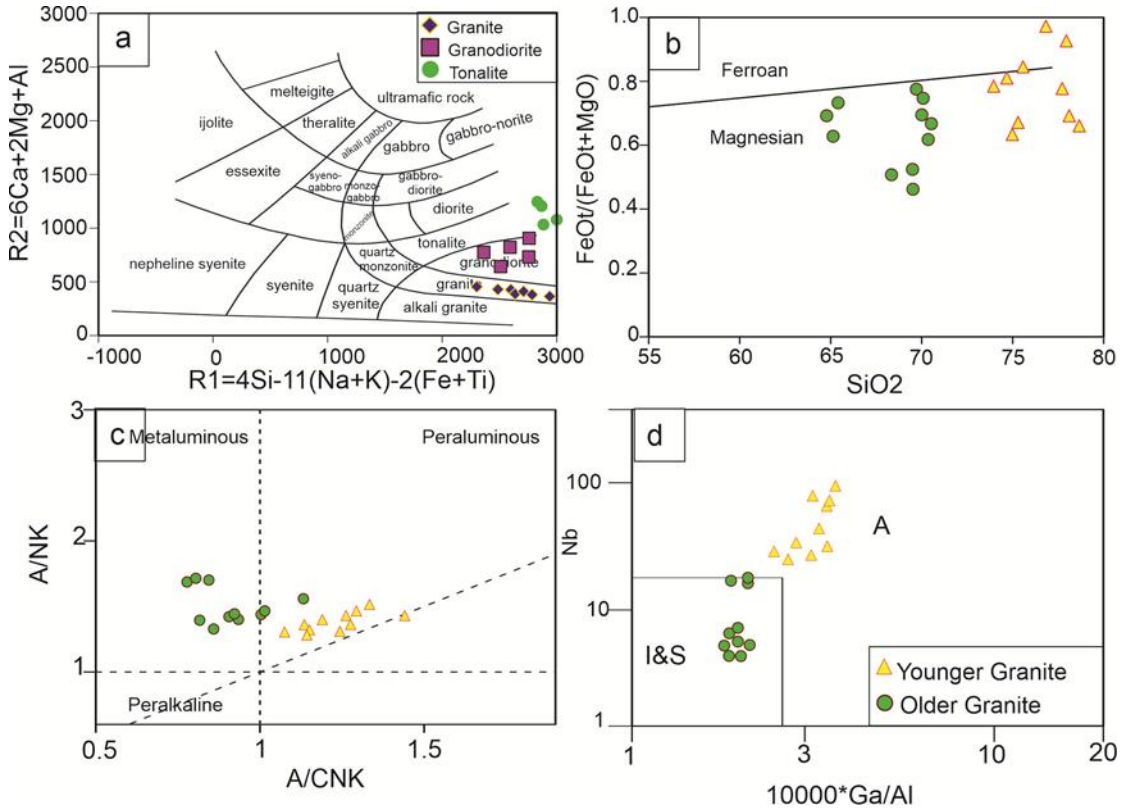

Fig. 8. For El Bariud granitic suite, geochemical discrimination was carried out using several classification plots: (a) the cation-based R1–R2 diagram of De la Roche et al. (1980); Data after Abuamarah et al. (2023). (b) FeOt/(FeOt + MgO) versus SiO_2 fields outlined by Frost et al. (2001) fields; Data after El Bialy and Omar (2015); (c) the molar ratio plot of A/CNK against A/NK (Maniar and Piccoli 1989), where A/NK = $Al_2O_3/(K_2O + Na_2O)$ and A/CNK = $Al_2O_3/(CaO + K_2O + Na_2O)$, field, Data after El Bialy and Omar (2015); and (d) Whalen et al. (1987) diagram showing 10^4 Ga/Al versus Zr; Data after Abuamarah et al. (2023).

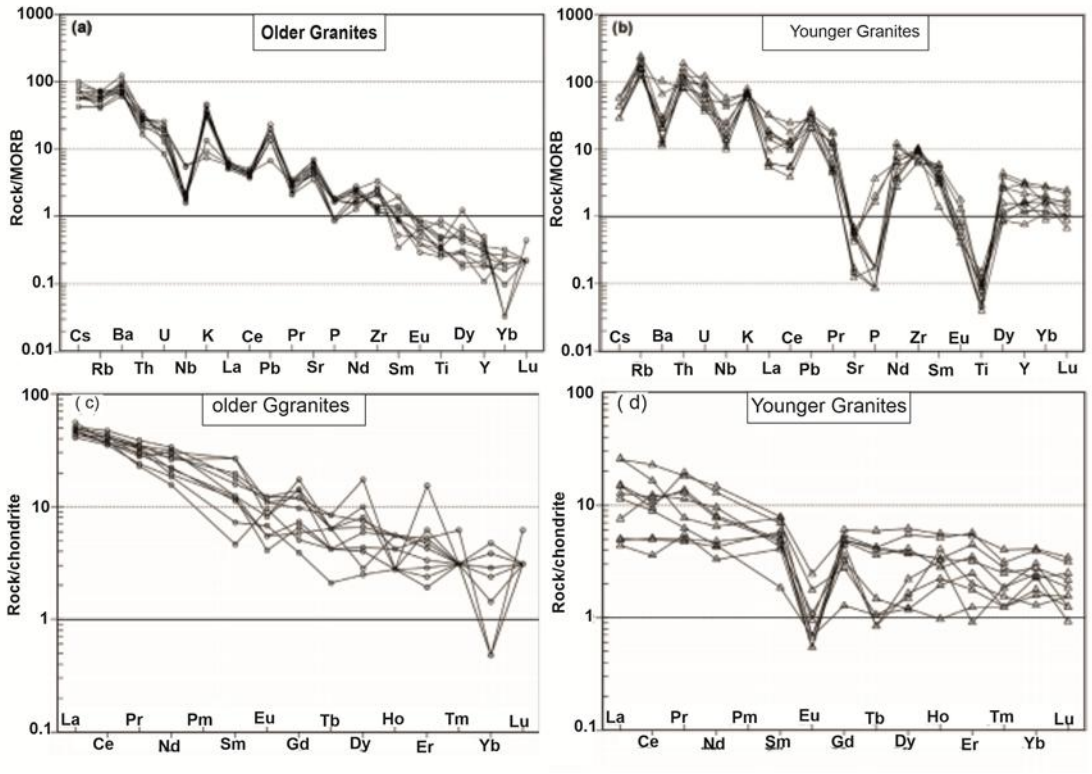

Fig. 9. Bulk-rock chemistry of Wadi Al Baroud .**a and b**) MORB-normalized multi-element spider Older and Younger Granites. Normalization values are from Sun and McDonough (1989). c and d Chondrite-normalized REE patterns of the investigated older and younger granites, chondrite values are from (McDonough and Sun, 1995). Data of wadi Baroud granitoids are from El Bialy and Omar (2015).

High Fe_2O_3 and TiO_2 in massive titaniferous ores reflect abundant titanomagnetite and ilmenite. Low LOI values, especially negative in ores, indicate reduced iron and sample freshness. Positive TiO_2–Fe_2O_3–Nb correlations resemble those in Panzhihua intrusion (Song et al., 2013). The titaniferous iron ores are enriched in trace elements like Mn, V, Cr, Zn, Ni, and Co, while the gabbroic rocks have high Ba contents, linked to plagioclase crystallization. Sc shows limited variation and no correlation with clinopyroxene (Rollison,, 1993). REE concentrations are low in iron ores (ΣREE: 2.25–24.5 ppm) but higher in host gabbros (ΣREE: 61–110 ppm), showing LREE enrichment and flat chondrite-normalized patterns, similar to Fe-Ti oxide ores from the Panzhihua intrusion. Primitive mantle-normalized REE patterns also align with those of Panzhihua, with slight positive Eu anomalies in gabbros (Zhou et al.,2005;Song et al., 2013).

Twelve representative whole-rock samples were analyzed geochemically from the Abu Hadieda reveals two distinct groups pyroxene-hornblende gabbros and diorites with variations attributed to mineral modal differences (Abdelfadil et al., 2022). Gabbros show higher TiO_2, Fe_2O_3*, and lower SiO_2 and alkalis, while diorites are more evolved with higher SiO_2, alkalis, and lower Fe-Mg-Ti contents (Abdelfadil et al., 2022). Both groups exhibit tholeiitic to transitional affinities with reveal high concentrations of incompatible elements coupled with distinct depletions in Ta and Nb, typical of arc-related magmas. REE patterns show strong LREE enrichment, moderate (La/Yb)N ratios, and Eu anomalies, reflecting amphibole fractionation (Abdelfadil et al., 2022). Such geochemical signatures are comparable to those of post-collisional intrusions elsewhere in the ANS (e.g., Abu Anbar, 2009; Ali et al., 2021; Khalil et al., 2015; Samuel et al., 2015).

Awad et al (2022a) studied the gabbroic rock in Abu Murrat Area, They used the Na_2O + K_2O vs. SiO_2 binary diagram (Cox, 2013), these samples clearly fall within the gabbro field, The AFM diagram (Irvine and Baragan, 1971) indicates a tholeiitic magma trend, while the Rb vs. Y+Nb plot (Pearce, 1984) places the gabbros within a volcanic arc tectonic setting. Trace element analysis shows that both the Fe-Ti oxide bearing gabbroic rocks and their mineral deposits are enriched with compatible trace elements like V and Co, with higher values in the mineralized zones. Incompatible elements (LILEs) such as Sr, Ba, and Rb are more abundant in the gabbro, while HFSEs like Zr and Nb are generally low in both rock types (Awad et al., 2022a). Zn and Pb are enriched, especially in mineralized samples. REEs are overall depleted, but LREEs are more enriched than HREEs, with higher total REE content in the Fe-Ti oxide mineralization. Normalization patterns indicate elevated levels of Pb, Ti, and Sr, alongside reduced concentrations of Th, Zr, and

Yb, with slight positive Eu anomalies. These trends suggest magmatic differentiation and mineral fractionation processes (Awad et al., 2022a)

We classified Abu Murrat gabbros into pyroxene, hornblende-bearing) and monzodiorite (leucogabbro) fields (Fig. 10a), while Fe-Ti-P-rich gabbros fall outside due to low SiO_2 content. Low LOI values characterize these samples (0.03–2.54 wt%), confirming their freshness, and exhibit low Mg# (0.22–0.44), similar to Fe-Ti-rich gabbros from Abu Ghalaga (Khalil et al., 2023). Major oxides vary widely especially in SiO_2, TiO_2, Fe_2O_3, Al_2O_3, and P_2O_5 contents are attributed to the prevalence of Fe-Ti oxides, apatite, and the fractionation of plagioclase. Leucogabbros contain higher Al_2O_3 and lower Fe_2O_3 and TiO_2, consistent with high plagioclase and minimal Fe-Ti oxides, while certain gabbroic samples (e.g., Bd28, Bd32, Bd69) are enriched in Fe_2O_3, TiO_2, and V due to increased Fe-Ti oxide content.

Fe-Ti-P ores are chemically distinct, having significantly lower silicate-related oxides (e.g., SiO_2, Al_2O_3, Na_2O) but enriched in Fe_2O_3 (up to 74.46 wt%), TiO_2, V, Cr, Co, and Ni, corresponding with their high magnetite and ilmenite contents. Semi-massive to massive ores contain more Fe-Ti oxides and trace metals than disseminated ones (Fig. 10b). Sample Bd95A (gabbro-nelsonite) is notably enriched in P_2O_5, CaO, and REEs due to abundant apatite.

The REE content varies with rock type: gabbros and ore layers show total REEs ranging from 35–347 ppm and 3–205 ppm, respectively, reflecting modal mineral composition, fractionation, and residual liquids. Leucogabbros contain lower REEs, Th, U, Nb, Zr, and Y than other gabbro types. Chondrite-normalized REE patterns show LREE enrichment over HREEs and minimal Eu anomalies (Fig. 11), except in two leucogabbros with positive Eu shifts, suggesting plagioclase accumulation.

Comparatively, Abu Murrat gabbros share REE patterns with layered intrusions like Sept Iles, Hongge, and Damiao (Namur et al., 2010; Luan et al., 2014; He et al., 2016), while Fe-Ti-(P) ores resemble those from the Damiao complex and Khamal nelsonites (He et al., 2016; Eldougdoug et al., 2020). Primitive mantle-normalized diagrams reveal enrichment in fluid-mobile elements (As, Ba, Sr) and depletion in elements such as Cs and Hf (Fig. 11b), indicating similar geochemical processes to those in layered intrusions such as Hongge.

5. Discussion

5.1. Granitic Rocks

5.1.1. Genetic type and tectonic setting signature

El Bialy and Omar (2015) suggested that the Older Granite suite at Wadi Al-Baroud shows geochemical traits typical of subduction-zone magmatism. These rocks exhibit calc-alkaline traits, showing enrichment in large-ion lithophile elements (such as Sr and Ba) alongside depletion in high field strength elements like Nb and Y, with strong negative Nb anomalies. Tectonic discrimination diagrams place these granitoids within volcanic arc settings, consistent with pre-collisional I-type granites formed at active continental margins. Conversely, the Younger Granite suite exhibits features of post-collisional, A-type granites, such as elevated Nb, Zr, and Hf levels, negative Ba anomalies, and high Y+Nb–Rb ratios. These features imply genesis during post-orogenic crustal extension following the Arabian–Nubian Shield's collision with West Gondwana.

Abuamarah et al (2023) classified the older granitic rocks at Wadi Baroud as syntectonic I-type granitoids with metaluminous and calc-alkaline characteristics. Their geochemical profile reflects a subduction zone influence, marked by increased LILE elements and decreased concentrations of high-field-strength elements such as Nb and Ta. Partial melting of mafic lower crust is the probable source of these granitoids, had previously undergone modification through earlier subduction processes, rather than being directly sourced from mantle melts, as evidenced by the absence of mafic equivalents. Conversely, the post-collisional granites (PCG) are A-type granites characterized by high concentrations of Nb, Zr, Hf, Th, and Y geochemical traits typical of within-plate tectonic settings while exhibiting mildly metaluminous to peraluminous compositions. The absence of associated mafic or intermediate rocks suggests they did not form through classical mantle-derived magma fractionation. Instead, their origin is best attributed to partial melting of juvenile I-type crust, such as calc-alkaline tonalites, rather than sedimentary sources. Their geochemical signatures, including low K/Rb and high Nb/Ta ratios, reinforce a crustal melt origin. Tectonically, these granites formed during the post-collisional phase of the ANS (approximately 620–590 Ma), following events like crustal thickening, slab break-off, and lithospheric delamination.

Finally, the study of granitic rocks indicates that the Older Granites are calc-alkaline, magnesian, metaluminous I-type granitoids whereas the Younger Granites are relatively richer in iron, vary from metaluminous to peraluminous, and exhibit alkaline to alkali-calcic characteristics typical of A-type granitoids.

Tectonic discrimination diagrams using trace element (e.g., Nb vs. Y, Rb vs. Y+Nb) indicate volcanic arc affinities for the Older Granites and within-plate signatures for the Younger Granites (El Bialy and Omar., 2015) (Fig. 12). The Younger Granites, particularly the monzogranites, show elevated rare metals (U, Th, Nb, Zr), high REE contents ΣREE (average = 232 ppm), low Sr, P, and MgO, and strong negative Eu anomalies (El Bialy and Omar, 2015). These features correspond to A1-type granitoids, interpreted to have formed in intraplate, anorogenic settings from mantle-derived magmas. The present study on the Abu Murrat granitoids shows consistent patterns, confirming similar tectonomagmatic affinities and compositional characteristics.

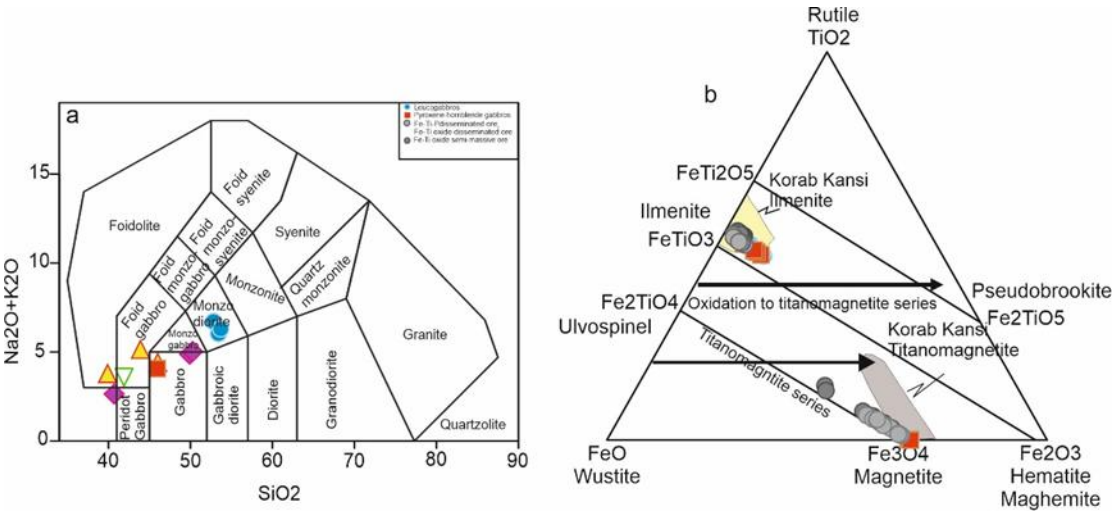

Fig. 10 . The bulk chemical data of the Abu Murrat gabbros are depicted through: (a) the Total Alkali-Silica (TAS) classification system outlined by Middlemost (1994), and (b) a ternary diagram of FeO, TiO_2, and Fe_2O_3 components for Fe–Ti oxide minerals following Buddington and Lindsley (1964). Comparative fields representing magnetite and ilmenite from the Korab Kansi region (Khedr et al., 2020) are highlighted in yellow and green

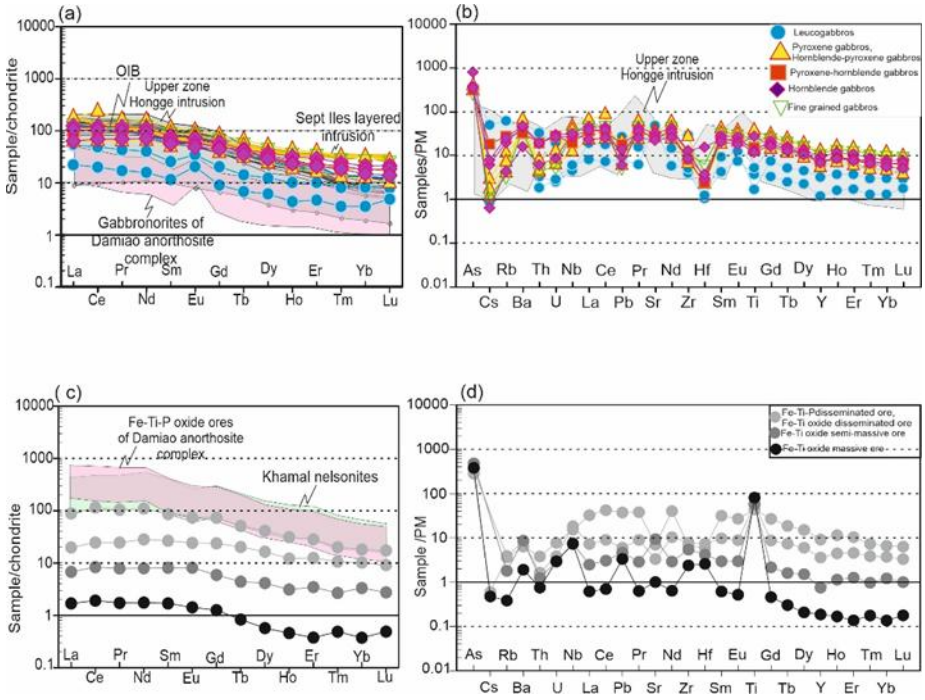

Fig. 11. The trace and rare earth element (REE) compositions of Abu Murrat gabbros and Fe-Ti-(P) oxide ores are displayed using: **(a, c)** C1 chondrite-normalized REE patterns, and **(b, d)** primitive mantle (PM)-normalized trace element patterns, with normalization data from McDonough and Sun (1995). These data are compared with similar signatures from well-known geological units like the Hongge intrusion, Sept Iles layered intrusion, Damiao anorthosite complex, Khamal Nelsonites, and ocean island basalts to understand their petrogenesis and tectonic setting (Luan et al. 2014;Namur et al. 2010; He et al. 2016; Eldoudouge et al. 2020; OIB; Sun and McDonough 1989) are used for comparison.

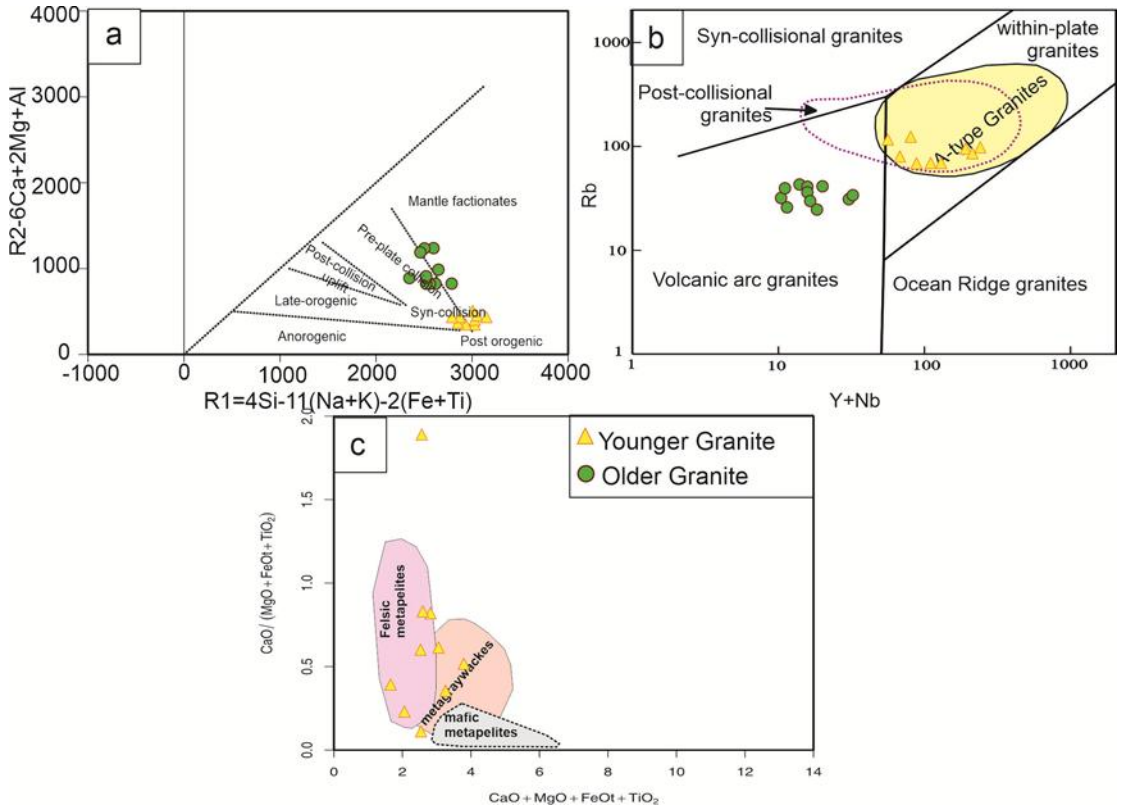

Fig. 12. Geochemical data for granitic rocks include: (a) R1–R2 tectonic discrimination diagram following Batchelor and Bowden (1985).; (b) Y + Nb against Rb diagram after Whalen et al. (1987), (c) a comparison of Younger Granites composition with experimental melt compositions from dehydration melting of metasedimentary and igneous rocks (Patino Douce. (1999).The plotted data of Wadi Al-Baroud granitic rocks are after El Bialy and Omar (2015).

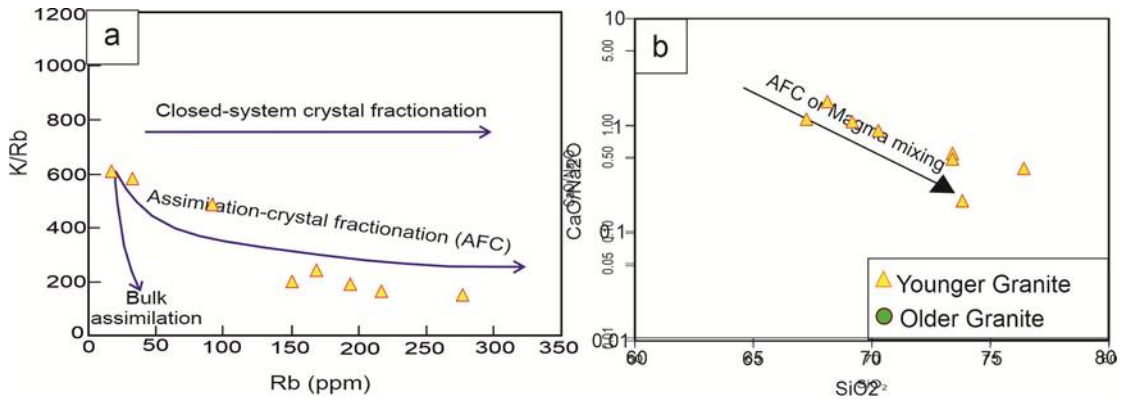

Fig. 13. a) Fractional crystallization and assimilation shown by Rb (ppm) versus K/Rb plot (El-Nisr and El-Sayed , 2001), b) CaO/Na_2O versus SiO_2 plot. AFC = assimilation fractional crystallization trends (Akinin et al., 2009). The plotted data are from El Bialy and Omar (2015).

5.1.2. Petrogenesis and nature of magma source

El Bialy and Omar (2015) suggested that the pre-collisional Older Granite suite at Wadi Al-Baroud is characterized by I-type, calc-alkaline arc-related granitoids, formed through mantle-derived magmas that underwent assimilation and fractional crystallization with crustal materials during ascent. Geochemical signatures (e.g., Rb/Sr, Ba/Rb, Th/Ta, Nb/Ta, Y/Nb) suggest input from both mantle and crustal sources. In contrast, the Younger Granite suite formed after the collision, representing A-type, peraluminous granites. They probably formed through partial melting of felsic metasedimentary rocks, especially psammite and pelite types due to post-collisional processes like lithospheric delamination and slab break-off. Their trace element patterns (e.g., enriched Zr and REEs, low CaO/Na_2O, Nb, Ti, and Eu) support a crustal origin rather than derivation from earlier I-type granites.

Abuamarah et al. (2023) studied wadi Baroud granitic rocks, they suggested that the petrogenesis of tonalite and granodiorite compositions, with minor interaction through magma mingling, evidenced by the existence of mafic microgranular enclaves (MMEs). Tectonically, they were emplaced during the active subduction phase of the ANS, prior to the continental collision, and their geochemical signature reflects melting of juvenile arc crust within a continental arc setting, where thermal input was provided by underplated mantle-derived magmas. On the other hand, the younger granites affected by these processes leading to crustal uplift, enhanced thermal input, and extension, which triggered melting in the lower crust. The emplacement occurred in an extensional regime, marked by doming, erosion, and the development of shear zones.

Geochemical evidence indicates that The Parental magmas of the Abu Murrat granites experienced extensive compositional changes due to various magmatic processes, particularly crustal contamination and fractional crystallization. Evidence for magma mixing and contamination is indicated by the presence of mafic xenoliths in the Older Granites (Fig. 2b). Geochemical ratios as (K/Rb, Ba/Nb, and Zr/Nb) in the Older Granites suggest strong crustal assimilation, as these ratios typically remain stable during simple fractional crystallization (Whalen et al., 1987; Azer et al., 2019). Monzogranites, with higher K/Rb values and Rb contents, display trends consistent with assimilation–fractional crystallization (AFC), whereas most Older Granites follow an assimilation-dominated path (Fig. 13a). The CaO/Na_2O versus SiO_2 trend further supports distinct AFC evolution in both granite types (Fig. 13b) which makes it compatible with Wadi Al-Baroud (El Bialy and Omar, 2015).

Plagioclase fractionation played a key role in magma evolution, evidenced by decreasing Sr and CaO with increasing SiO_2 and supported by $Zr–TiO_2$ trends. Monzogranites exhibit strong negative Eu, Sr, and Ba anomalies (Fig. 9b), indicating significant plagioclase removal, whereas the weaker Eu anomaly in Older Granites suggests limited plagioclase fractionation (Fig. 9a). Decreasing Fe_2O_3 and MgO with increasing SiO_2 reflects ferromagnesian silicate fractionation, while negative P_2O_5, TiO_2, and V with SiO_2 correlations and P–Ti depletions (Fig. 9b) point to apatite and Fe–Ti oxide separation. Positive K_2O and Rb trends with SiO_2 in monzogranites may indicate K-feldspar accumulation. Elevated FeO/MgO ratios in both granite suites and REE patterns with LREE enrichment over HREE (Fig. 9b) are consistent with fractional crystallization as a dominant process. Geochemical and petrogenetic data suggest magma derivation from both mantle and crustal sources: Older granitoids (diorite, tonalite) formed through fractional crystallization of mantle magmas with crustal assimilation, whereas Younger Granites likely resulted from partial melting of earlier crustal rocks, influenced by mantle-derived mafic magmas (Fig. 12c).

5.1.3. Radioelements Potentially

Radiogenic isotopes such as Nd and Hf are widely used to constrain the sources of granitic magmas. However, because the ANS at the time of emplacement of both the Older and Younger Granite suites consisted largely of newly formed juvenile crust, distinguishing between crustal and mantle contributions using isotope data alone is challenging (Stein and Goldstein, 1996; Abdelsalam and Stern, 1996; Eyal et al., 2004, 2010; Moussa et al., 2008; Morag et al., 2011). Numerous investigations combining U–Pb zircon ages with Nd isotope analyses from igneous and metamorphic rocks across the ANS have consistently indicated derivation from variably depleted mantle sources (e.g., Stern and Gottfried, 1986; Dixon and Golombek, 1988; Stein and Goldstein, 1996; Moghazi et al., 1998; Stern, 2002; Moussa et al., 2008; Andresen et al., 2009; Stern et al., 2010; Ali et al., 2009; Liégeois and Stern, 2010). Therefore, quantifying the relative proportions of crustal versus mantle inputs in these granitic magmas remains problematic. In the subsequent discussion, we use whole-rock geochemical data to evaluate the possible contributions of crust and mantle in the genesis of the Wadi Al-Baroud granitoids.

Pre-collision (arc) Older Granite suite

Volcanic arc granites generally originate from depleted mantle modified by subduction inputs of oceanic crust and sediments (Pearce, 1996). The calc-alkaline I-type granitoids of the Wadi Al-Baroud Older Granite suite likely incorporated melts from mantle, subducted components, and minor crustal material (e.g. Hildreth and

Moorbath, 1988; Defant and Drummond, 1993; Atherton and Petford, 1993; Miller et al., 2001; Castillo and Newhall, 2008). The subduction flux mainly introduced volatiles and LILEs, while crustal input was added during magma ascent (Gill, 1981;

Hawkesworth et al., 1991; Pearce and Peate, 1995). Their low initial $^{87}Sr/^{86}Sr$ ratios (0.702–0.704) (Rogers et al., 1978; Dixon, 1981; Stern and Hedge, 1985; Abdel-Rahman and Doig, 1987) and consistently low Rb/Sr values (0.04–0.11; avg. 0.07) (El Bialy and Omar., 2015) indicate a strong mantle influence, since mantle sources typically show much lower Rb/Sr than continental crust. The Ba/Rb ratios of the I-type Older Granites (10.33–20.1; avg. 15.98; El Bialy and Omar., 2015) are close to mantle estimates (Ba/Rb ≈11; Hofmann and White, 1983) but significantly higher than typical crustal values (≈6.7; Rudnick and Fountain, 1995). Their Th/Ta ratios (4.14–21.5; avg. 7.15; El Bialy and Omar, 2015) suggest contributions from crustal materials, since mantle-derived melts typically yield values near 2, whereas continental crust averages much higher. The Nb/Ta ratios of these granitoids are super chondritic (avg. 21.81; El Bialy and Omar, 2015), consistent with mantle source, while Y/Nb ratios show a mixed signal: most samples exceed 1.2 (crustal origin) (Eby, 1990, 1992), though a few remain below 1.2 (mantle affinity). Collectively, these data imply that the parental magmas incorporated both mantle and crustal components, typical of continental arc settings (El Bialy and Omar, 2015). Such hybrid signatures are most plausibly explained by assimilation–fractional crystallization (AFC), whereby mantle-derived magmas evolve through

concurrent crystallization and assimilation of crustal material during ascent and storage. Petrographic evidence, such as oscillatory zoned plagioclase, further supports open-system processes during the evolution of the Older Granite suite. The Wadi Al-Baroud Older Granites did not evolve by simple closed-system fractionation. Trace element ratios (Th/Nb vs. Zr; K/Rb, Ba/Nb, Zr/Rb vs. SiO_2) indicate that crustal assimilation accompanied fractional crystallization (AFC). Strong negative Nb anomalies further confirm contamination by crustal material during magma evolution.

Post-collisional Younger Granite suite

High-K calc-alkaline A-type granites in post-collisional environments are commonly linked to partial melting of crustal materials, triggered by processes such as slab breakoff and lithospheric delamination (Davies and von Blanckenburg, 1995; Schott and Schmeling, 1998; Sperner et al., 2001; Moghazi, 2003; Avigad and Gvirtzman, 2009; El-Bialy, 2010; Ali et al., 2013; Eliwa et al., 2014). Similar interpretations have been proposed for many Younger Granite intrusions in the Eastern Desert and Sinai, which likely developed during a tectonic transition from compression to extension (Moghazi et al., 1999, 2004; Katzir et al., 2007; Moussa et al., 2008; El-Bialy and Streck, 2009; Eyal et al., 2010; Farahat et al., 2011; Azer, 2013; Eliwa et al., 2013). The Wadi Al-Baroud Younger Granites, being strongly peraluminous (A/CNK ≈ 1.13), also point to a predominantly crustal origin. Their enrichment in alkalis, Rb, Pb, Th, and REE, together with strong negative Nb, Ti, P, Sr, and Eu anomalies, further supports melting of metasedimentary protoliths coupled with advanced differentiation.

Possible petrogenetic models include: (1) melting of metapelitic or metagreywacke sediments, occasionally involving basaltic input; (2) partial melting of tonalitic–granodioritic crust with amphibole/pyroxene residues; or (3) differentiation of primitive granites by amphibole fractionation. Geochemical signatures of the Wadi Al-Baroud samples, such as low CaO/Na_2O ratios (0.39 on average), elevated Zr contents, and high zircon saturation temperatures (~935 °C), are most consistent with extensive melting of pelitic–psammitic sediments. This rules out the nearby I-type Older Granites as sources. Instead, abundant Al-rich metasediments in the Eastern Desert and Sinai provide the most plausible parent material. Comparable crustal sources have also been documented for other peraluminous granites in southern Egypt (Moghazi et al., 2004; Gharib, 2012). Therefore, partial melting of metasediments is the most likely process behind the Wadi Al-Baroud Younger Granites, whereas alternative models may explain other members of the Younger Granite suite in the region.

5.2. Gabbroic Rocks

5.2.1. Pressure-temperature conditions and oxygen fugacity

Abdelfadil et al (2022) studied Abu Hadieda gabbros suggesting that Crystallization pressures derived from Al-in-hornblende geobarometers indicate that the pyroxene-hornblende gabbro intruded at mid-crustal depths (~18 km, 0.6 GPa), These differences point to magma ascent during evolution. Pyroxene chemistry plots near the Skaergaard trend, typical of shallow-level differentiation, confirming low-pressure crystallization. Geothermometry using apatite saturation and clinopyroxene-amphibole thermometers estimates crystallization temperatures of 900–1028 °C for gabbros, consistent with their compositional maturity. Amphibole and biotite analyses reflect moderately oxidizing to mildly reducing magma conditions, with $\log fO_2$ values ranging from −12.9 to −13.6. These redox states, near the quartz-fayalite-magnetite (QFM) buffer, resemble those of mid-ocean ridge basalts and are more reducing than typical modern arc magmas—possibly indicating distinct oxidation conditions in Proterozoic arc settings.

Khedr et al (2024) about gabbro, in El Baroud area, they suggested that Clinopyroxene crystallized between 800–1000 °Cat pressures of 1.5–3.0 kbar, corresponding to depths <12 km. Cpx compositions also confirm high fO_2 during formation. Thus, the El-Baroud intrusion likely formed under oxidized, hydrous, mid-crustal conditions common among similar mafic bodies in the Eastern Desert of Egypt.

The chemical composition of plagioclase in the Abu Murrat gabbros and Fe-Ti-P oxide ores indicates crystallization temperatures of ~950–1110 °C on the Ab-An-Or diagram (Fig. 14a ;Fuhrman and Lindsley 1988). The isothermal lines depicted on the Wo-En-Fs diagram of pyroxene (Fig. 14b; Lindsley 1983; Morimoto et al. 1988), Pyroxene thermometry shows a broader temperature range of ~800–1200 °C, suggesting prolonged crystallization, while Cpx diagrams (Fig.14c ;Soesoo 1997) restrict temperatures to ~1100–1150 °C. Temperatures estimated from twenty coexisting Cpx–Opx pairs in the Abu Murrat gabbros and their associated Fe-Ti-P oxide ores range between 944°C and 1162°C, calculated using the thermometric equation (36) of Putirka (2008). Similarly, applying the equations of Brey and Köhler (1990) to these pairs produced comparable values, spanning 826–1120°C.

Amphibole chemistry provides additional insights into temperature, pressure, and oxygen fugacity. Ti and Al^{iv} contents correlate positively with crystallization temperature, giving average values of ~921 °C (Helz 1973; Ridolfi et al. 2010). Fe-biotite crystallized late at lower temperatures (670–700 °C; Henry et al. 2005).

The analyzed primary amphiboles exhibit an Al^{iv}/Al^{vi} ratio exceeding 3, suggesting crystallization at relatively low pressures of less than 5 kbar (Fig. 14d ;Fleet and Barnett 1978). Application of the barometric calibrations proposed by Hammarstrom and Zen (1986), Hollister et al. (1987), Anderson and Smith (1995), and Johnson and Rutherford (1989) yields an average pressure of about 5.4 kbar, equivalent to an emplacement depth near 18 km (SI: Table S1). Furthermore, clinopyroxene compositions plotted on the XPT–YPT diagram (Soesoo 1997; Fig. 14e) point to pressures between < 2 and ~5 kbar.

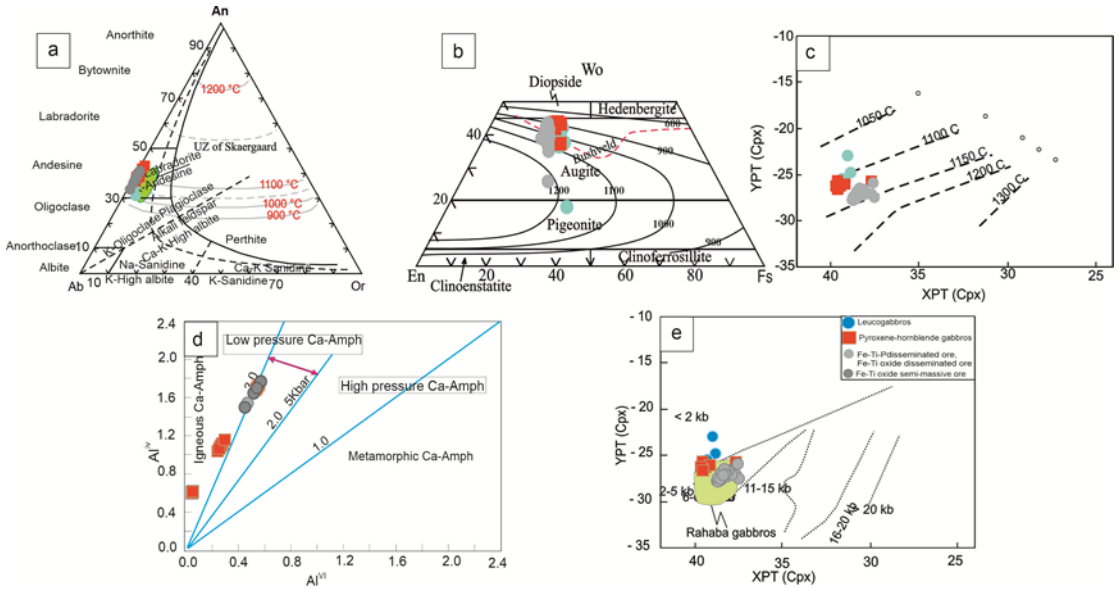

Fig. 14. Mineral chemistry of silicate minerals in the Abu Murrat gabbroic rocks and the hosted Fe-Ti-(P) oxide ores. **a)** Ab-An-Or triangular classification diagram of plagioclase (Ribbe, 1983). Field of plagioclase in the upper zone of skaergaard is used for comparison (Namur et al., 2014; Jang and Naslund, 2001). **b**) Wo-En-Fs nomenclature diagram of Cpx (Morimoto et al., 1988). The isothermal lines are after Stromer Jr. (1983) and the dashed red line indicates the Bushveld trend (Atkins, 1969). **c and e)** XPT vs. YPT diagram of clinopyroxene crystallization temperature and pressure (Soesoo, 1997). **d)** Alvi vs. Aliv variation diagram showing differences between igneous and metamorphic amphiboles (Fleet and Barnett, 1978).

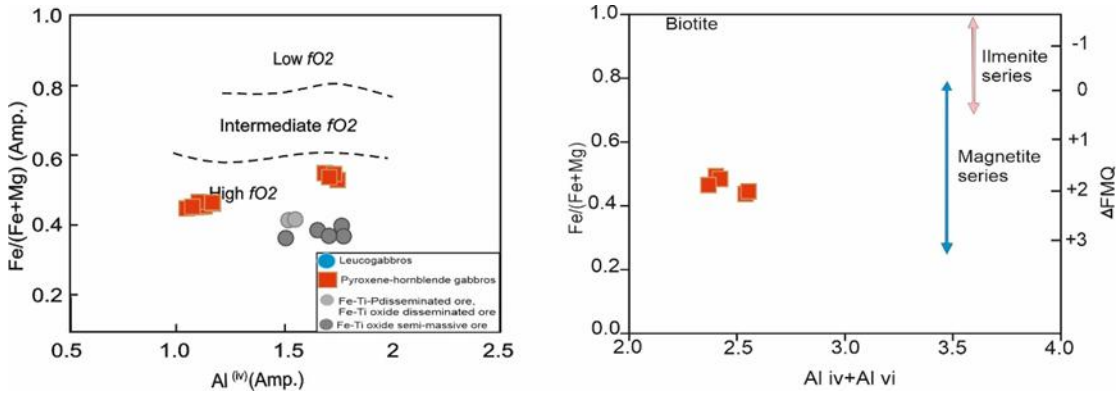

Fig. 15. Geothermobarometry of the Abu Murrat gabbroic rocks. **a)** Aliv vs. Fe/Fe + Mg of primary amphiboles showing *fO2* conditions (Anderson and Smith, 1995).**b)** Aliv + Alvi vs. Fe/(Fe + Mg) of biotite. Ilmenite and magnetite series is after Anderson et al. (2008).

The relatively low Fe/(Fe+Ti) ratios observed in the studied primary amphiboles suggest crystallization under elevated oxygen fugacity (fO_2) conditions (Anderson and Smith 1995) (Fig. 15a). Oxygen fugacity estimates from biotite (Fe ratios) indicate oxidizing conditions between QFM +1.7 and +2.2 (Anderson et al., 2008) (Fig. 15b). The dominance of titanomagnetite over ilmenite and low V content (V_2O_3: 0.07–0.45 wt%) observed in the analyzed magnetite (SI: Table S2, Table S1) indicates crystallization under high fO_2 conditions, as V acts as an incompatible element in magnetite under relatively oxidizing environments (Charlier et al. 2009). Early magnetite inclusions in Cpx also point to $fO2$ > FMQ +2, Toplis and Carroll 1995).

Magnetite–ilmenite thermometry (Lepage 2003; Lattard et al. 2005) yields lower re-equilibration temperatures of 461–679 °C and 496–679°C, respectively, while spinel–titanomagnetite intergrowths suggest crystallization below 600 °C (Fig. 6(c, f, i, l; Turnock and Eugster 1962). Calculated fO_2 values from ILMAT show log fO_2 ranges of –18.69 to –16.35 (gabbros) and –24.33 to –18.2 (Fe-Ti-P ores). These represent solidus re-equilibration rather than direct magmatic conditions. High oxygen fugacity inhibited significant sulfide mineralization during ore formation.

5.2.2. Genetic type and tectonic setting signature

Khedr et al. (2024) reported that El-Baroud mafic intrusion originated from ferropicritic magmas derived through partial melting of a metasomatized lithospheric mantle source enriched in Rb, Ba, Sr, Pb, and LREE. This enrichment likely resulted from interaction with mantle plumes or during asthenospheric upwelling. Mixing with minor plume- or asthenosphere-derived melts likely contributed additional Fe, Ti, Nb, and Ta, as reflected in the high HFSE content of both the gabbroic host and Fe-Ti ores. The Fe-Ti oxides developed as a result of both crystallizing directly within the rock and separation of an immiscible liquid phase, leading to layered and disseminated textures within the host gabbros. The formation of thick Fe-Ti oxide lenses is attributed to a combination of factors: the Fe-Ti-rich composition of the parent magma, elevated fO_2, high volatile content, and structural controls associated with the NW–SE Najd fault system. Additionally, the observed southward increase in Fe-Ti mineralization across the Eastern Desert may reflect more pronounced mantle plume activity and structural deformation in the SED relative to NED.

Through our study, the Abu Murrat gabbros represent a highly evolved, post-tectonic layered mafic intrusion derived from ferrobasaltic mantle melts (Fig. 16a,b). Field, petrographic, and geochemical evidence indicate advanced magmatic fractionation, reflected in low Mg#, Ni, and Cr values, and enrichment in Fe, Ti, and P. Cumulate textures, rhythmic layering, and the concentration of apatite and Fe-Ti-P oxides in the upper zones resemble global layered intrusions. Plagioclase (An31–43), clinopyroxene, and amphibole compositions confirm the evolved nature of the magma. Elevated REE, Zr, Th, and (La/Sm)N ratios, along with xenoliths and amphibole/biotite chemistry, indicate significant crustal contamination. The parental magma is ferrobasaltic, lacking olivine olivine in the Abu Murrat gabbroic lithologies, along with their low MgO contents (1.35-5.69 wt%) does not indicate that ferropicrites served as parent melts. Ferrodiorites or jotunites serve as parent melts for significant anorthosite complex, including the Damiao and Rogaland anorthosite complexes (Duchesne and Liégeois 2015; He et al. 2016). No anorthosite was observed in the studied area, thus ferrodiorites can be excluded as parent melts. The ferrobasaltic parent melt aligns well with the studied Abu Murrat gabbros Fig. 16 a, b). SiO_2 content is low (~ 41 wt%), while FeO_t (~ 18 wt%) and TiO_2 (~ 4.5 wt%) are highly enriched. Additionally, the samples show moderate enrichment in trace elements and relatively fractionated REE patterns, with most samples lacking positive Eu anomalies (Fig 11a and b); SI: Table S3). These features align with the ferrobasaltic parent melt composition of the Sept Iles layered intrusion (Namur et al. 2010). The low Mg# (0.22–0.44) of the Abu Murrat gabbros indicates a characteristic of ferrobasaltic magma (Mg#: 0.28–0.46; Brooks et al. 1991). The chondrite-normalized REE patterns of Abu Murrat gabbros closely resemble those of fine-grained mafic samples from the chilled margin of the ferrobasaltic Sept Iles layered intrusion (Namur et al. 2010) (Fig. 11a). consistent with melts formed through deep, high-pressure fractionation of a garnet-bearing plume source. Tectonic discrimination diagrams place the gabbros in within-plate, rift-related fields. The Abu Murrat gabbroic samples plot within the ocean island basalt (OIB) field on the DF1–DF2 binary discrimination diagram of Agrawal (2008) (Fig. 16c), pointing to a notable role of the asthenospheric mantle in producing Fe- and Ti-rich parental melts. These gabbros, together with the associated Fe-Ti oxide mineralization, are enriched in HFSE (e.g., Nb, Ti) as well as Fe (Fig. 11d), consistent with derivation from plume-related magmatism (Barbero et al., 2020). Their REE-normalized profiles are steep and match typical OIB signatures (Fig. 11a). The Abu Murrat gabbros show LaN/NdN ratios between 0.9 and 1.7 and SmN/YbN ratios from 3.1 to 4.7 (SI: Table S3), suggesting an enriched plume source containing residual garnet, comparable to the Fe-Ti basalts of the Duarte Complex in the northeastern Caribbean (LaN/NdN: 1.4–2.0; SmN/YbN: >3; Escuder-Viruete et al., 2007). Such LREE-rich Fe-Ti basalts, including the inferred Abu Murrat parental magma, are thought to arise from low-degree (<3%) partial melting of a heterogeneous deep-seated plume (Escuder-Viruete et al., 2007). Low-Mg tholeiitic basalts, like those of Abu Murrat, are typically generated by partial melting within the plume head under conditions of adiabatic decompression (Campbell et al., 1989). OIB formed beneath thick lithosphere generally display greater enrichment in Fe, Ti, and P compared to those emplaced beneath thin lithosphere (Humphreys and Niu, 2009). Accordingly, the Abu Murrat gabbroic intrusion is interpreted to have crystallized within a thicker lithospheric segment, where Fe and Ti enriched melts could concentrate and give rise to the formation of Fe-Ti oxide ores. Their crosscutting relationships with the surrounding granitoids indicate an age of approximately 630 to 610 Ma, comparable to post-tectonic gabbros of the Arabian-Nubian Shield (ANS) formed during the late Cordilleran stage (655–570 Ma) in the evolution of the ANS (e.g., Abu Anbar 2009; Azer and El-Gharbawy, 2011). Overall, the Abu Murrat gabbros reflect plume-driven magmatism in a post-collisional rift setting, with Fe-Ti-P enrichment facilitated by crustal interaction and extensive fractionation.

5.2.3. Genesis of Abu Murrat Fe-Ti-P oxide ores

Through our study, several mechanisms have been proposed for oxide precipitation from mafic magmas (Kolker, 1982; Duchesne, 1999). The main debate is whether Fe–Ti oxides form early during fractionation (Pang et al., 2009; Song et al., 2013; Bai et al., 2012) or later by liquid immiscibility (Zhou et al., 2005; Liu et al., 2016; Wang et al., 2021). At Abu Murrat, field and petrographic evidence stratiform oxide layers, sharp contacts with gabbros (Fig. 4c), and the coexistence of magnetite, ilmenite, silicates, and hornblende support precipitation from immiscible oxide-rich melts. Fe–Ti ores occur mainly in the lower intrusion, whereas Fe–Ti–P gabbro-nelsonites are concentrated near the top, consistent with late-stage evolved melts enriched in apatite (Bindeman et al., 1998). Textural relations, apatite abundance, and disseminated

sulfides suggest P and S acted as fluxing agents promoting immiscibility.

Geochemical data also record multiple stages of oxide formation. Semi-massive ores, poor in apatite (Fig. 6h, k), crystallized earlier at lower fO_2 (–21.81; Fe^{3+}/Fe^{2+} = 1.37), while Fe–Ti–P ores formed later from evolved melts under more oxidizing conditions (–22.34; Fe^{3+}/Fe^{2+} = 1.58). Cr-poor titanomagnetite (<0.2 wt% Cr_2O_3) further supports derivation from evolved immiscible Fe–Ti–(P) melts (Wang and Zhou, 2013), in contrast to Cr-rich oxide ores such as those at Korab Kansi (Khedr et al., 2022). The assemblage of Cr-poor oxides, ilmenite, apatite, and hornblende resembles immiscible systems like Hongge (Wang et al., 2021).

Bulk-rock chemistry indicates bimodality between silica-rich leucogabbros (high SiO_2, low FeOt) and Fe-rich ferrogabbros (low SiO_2, high FeOt, TiO_2, and P_2O_5), supporting melt unmixing (Charlier and Grove, 2012). Elevated TiO_2, P_2O_5, alkalis, and low MgO favor immiscibility (Visser and Koster van Groos, 1979; Bogaerts and Schmidt, 2006; Charlier and Grove, 2012). Textural evidence (poikilitic hornblende, biotite) and crystallization conditions (800–1150 °C; 2–5 kbar) indicate immiscibility at shallow depth under hydrous conditions, where elevated H_2O and fO_2 expanded the immiscibility field and enhanced magnetite precipitation (Carmichael and Ghiorso, 1986; Hou et al., 2018; Lester et al., 2013). Ferrogabbros are enriched in HFSE, REEs, and transition metals relative to leucogabbros. Overall, the Fe–Ti–(P) ores crystallized from immiscible late-stage melts, comparable to Skaergaard, Bushveld, Hongge, Sept Iles, and Abu Ghalaga intrusions (Jang and Naslund, 2001; Song et al., 2013; Luan et al., 2014; Namur et al., 2014; Wang et al., 2021; Khalil et al., 2023). When plotted on the Roedder (1951) liquid immiscibility diagram, most Abu Murrat samples fall within the two-liquid field (Fig. 17a). Similarly, in the Na2O+K2O–FeOt–MgO ternary diagram of Philpotts (1979), the samples lie within the immiscibility field, showing affinities with Emeishan LIP gabbros (Zhou et al., 2013) (Fig. 17b). A noticeable compositional gap further distinguishes the silica-rich and Fe-rich liquid trends. Crustal contamination likely aided the development of immiscible Fe–Ti–P liquids during magma ascent.

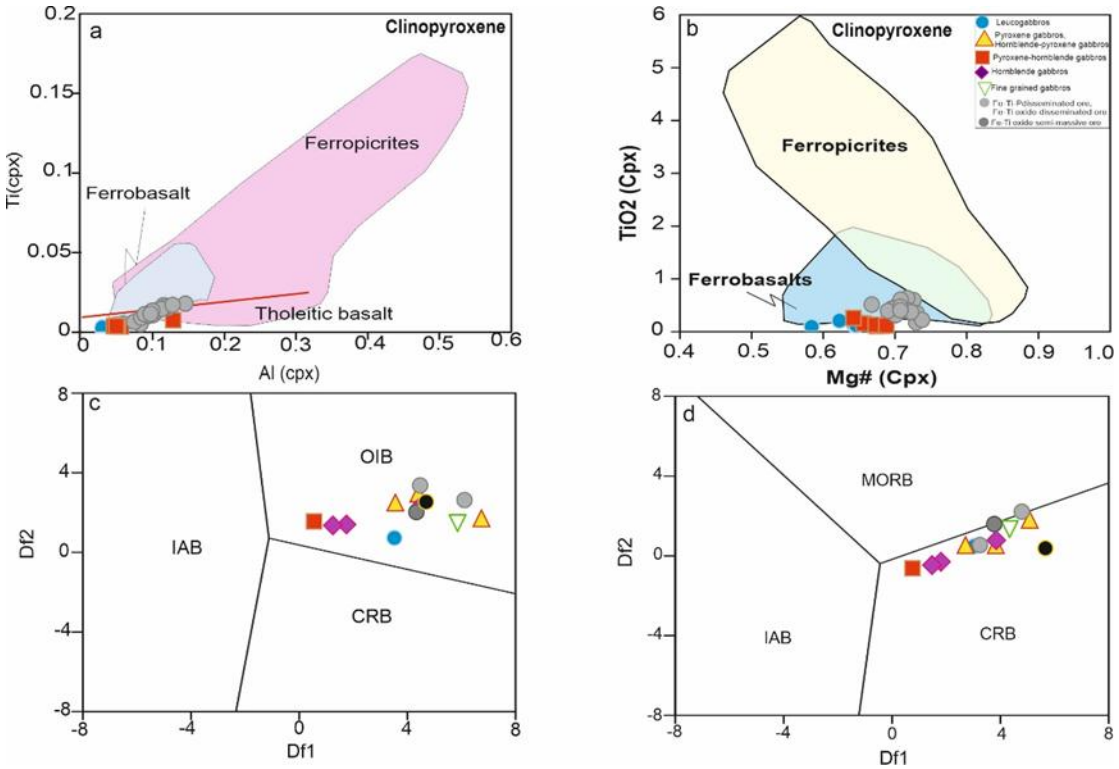

Fig. 16. a) Plot of aluminum (Al_t) versus titanium (Ti) concentrations in clinopyroxene from Abu Murrat (Leterrier et al., 1982). b) Diagram showing the relationship between magnesium number (Mg#) and TiO_2 content in Abu Murrat clinopyroxene. Fields for ferropicrite clinopyroxene are adapted from Gibson et al. (2000), Tuff et al. (2005), and Desta et al. (2014), while the ferrobasalt clinopyroxene field follows Lustrino (2006) and Namur et al. (2012). c, d) Tectonic discrimination diagrams (DF1 versus DF2) from Agrawal et al. (2008), classifying rock types as island arc basalt (IAB), continental rift basalt (CRB), mid-ocean ridge basalt (MORB), and ocean island basalt (OIB). The discriminant functions are:

DF1 = 0.3518 × ln(La/Th) + 0.6013 × ln(Sm/Th) - 1.3450 × ln(Yb/Th) + 2.1056 × ln(Nb/Th) - 5.4763
DF2 = -0.3050 × ln(La/Th) - 1.1801 × ln(Sm/Th) + 1.6189 × ln(Yb/Th) + 1.2260 × ln(Nb/Th) - 0.9944

5.2.4. Geochronology Synthesis of the Abu Murrat Igneous Rocks

The Neoproterozoic tectonic history of the ANS, especially within Egypt's NED, is generally divided into pre-collisional, syn-collisional, and post-collisional stages. Accurate crystallization ages of the different lithological units are essential for reconstructing these events. The Table 1 below compiles available U–Pb ages for the Older Granites, Younger Granites, and layered gabbroic intrusions from the Wadi Al-Baroud area and neighboring parts of the ANS, drawing on published sources.

The Older Granites are linked to arc-related and collisional magmatism, characterized by I-type calc-alkaline chemistry resulting from mantle-derived melts interacting with crustal material (Pearce, 1996). The Younger Granites formed during the post-collisional extensional stage, produced by partial melting of metasedimentary sources and intruding earlier granitoids with distinct contacts (El Bialy and Omar, 2015). Younger gabbros, including the ilmenite-bearing variety at Abu Murrat, crystallized in a late- to post-orogenic extensional regime from a subduction-modified mantle; however, precise dating for Abu Murrat is lacking and their ages are inferred from regional analogues.

Table 1: Geochronological of Major Rock Units in Wadi Al-Baroud and nearby regions

Rock Units	Crystallization Age Range(Ma)	Main Dating Methods	Tectonic Context
Older Granites (I-type)	850-615 Ma	Zircon U–Pb, Rb–Sr, K–Ar (various)	Pre-collisional stage; related to active continental margin subduction and arc magmatism. Developed through assimilation–fractional crystallization (AFC) of mixed crustal–mantle magmas ((Hussein et al., 1982; Stern and Hedge, 1985; Hassan and Hashad, 1990; Stern, 1994; Kroner et al., 1994; Moghazi, 2002; Moussa et al., 2008; El Mahallawi and Ahmed, 2012; El Bialy and Omar., 2015)
Younger Granites(A-type)	605–595 Ma (general 610–590 Ma)	Zircon U–Pb	Post-collisional stage; following collision between the juvenile Arabian–Nubian Shield crust and older West Gondwana terranes. Characterized by crustal extension and alkaline magmatism, derived from high-degree partial melting of metamorphosed sedimentary sources under high-T and reducing conditions (Stern and Hedge, 1985; Hassan and Hashad, 1990; Beyth et al., 1994; El-Sayed and El-Nisr, 1999; Moghazi, 2002; El-Sayed et al., 2002; Farahat et al., 2007, 2011; Mohamed and El-Sayed, 2008; Moussa et al., 2008; Ali et al., 2012, 2013; El Bialy and Omar., 2015)
Layered/Younger Gabbro Intrusions	~630–550 Ma (post-collisional gabbros)	(no U–Pb zircon or baddeleyite ages reported for Abu Murrat/Wadi Al-Baroud; inferred from analogous intrusions and field relations)	Post-collisional (arc-rift setting); emplaced after the older granitoids and contemporaneous with or slightly before younger granites. Originated from lithospheric mantle previously modified by subduction-related magmatism, later re-melted during crustal thinning and extension El Bialy and Omar., 2015)

5.2.4. Genetic model of Abu Murrat area

Previously mentioned geochemical features of the Abu Murrat Older and Younger Granites indicate that the Abu Murrat granitoids (Older and Younger) were crystallized in two distinct magmatic stages during the evolution of the ANS, reflecting the tectonic transition from a compressional (volcanic arc) setting to a post-compressional (extensional) environment (e.g., Azer et al., 2019; Seddik et al., 2020; El-Awady et al., 2024), (Fig. 18).

Granite magmatism at Abu Murrat likely began with calc-alkaline I-type granodiorites emplaced in a volcanic arc during early arc accretion along the East Gondwana margin (Fig. 18a). Slab-derived fluids probably triggered melting in the mantle wedge, producing basaltic magmas that stalled at the crustal base, where they induced partial melting and assimilation of lower crustal rocks. These processes generated the quartz-diorites, tonalites, and granodiorites of the Older Granite suite via differentiation and crustal interaction (Fig. 12b), as supported by Rb–K/Rb trends indicating AFC processes (Fig. 13a).

The layered gabbro at Abu Murrat, hosting Fe–Ti–(P) oxide ores, was emplaced in a post-collisional rift environment generated by lithospheric thinning and the ascent of mantle-derived ferrobasaltic magmas. Magmatic evolution involved fractional crystallization, crustal assimilation, and liquid immiscibility, which enriched the melts in Fe, Ti, and P and produced a zoned intrusion: ferrogabbros and Fe–Ti–P oxide ores crystallized from the Fe-rich immiscible melt at lower levels, while Si-rich melts formed leuogabbros at the top (Fig. 17c). The Fe–Ti–P ores developed mainly through liquid immiscibility, promoted by a distinctive magma chemistry with high TiO_2 (up to 7.64 wt%), P_2O_5 (5.46 wt%), alkalis (Na_2O+K_2O = 6.57 wt%), and low MgO (5.69 wt%), which lowered melt viscosity and expanded the immiscibility field. This process is reflected in the bimodal composition of the intrusion: silica-rich leuogabbro (SiO_2: 52.45 wt%, FeOt: 7.13 wt%) versus Fe-rich gabbro (SiO_2: 44.65 wt%, FeO_t: 14.55 wt%, TiO_2: 3.6 wt%, P_2O_5: 3.08 wt%). Immiscibility is further confirmed by the position of samples within the two-liquid fields of Roedder (1951) and Philpotts (1979) (Fig. 17a, b). Strong fractionation (Mg#: 22–44, Cr: 42–110 ppm, Ni: 10–43 ppm), the destabilizing effect of P on magnetite, crustal contamination, and high H_2O–fO_2 conditions collectively enhanced Fe–Ti–P enrichment, favored early magnetite crystallization, and promoted HFSE enrichment. Overall, the geochemical affinity with OIB and similarities to global layered intrusions suggests a plume-related extensional origin for the Abu Murrat complex.

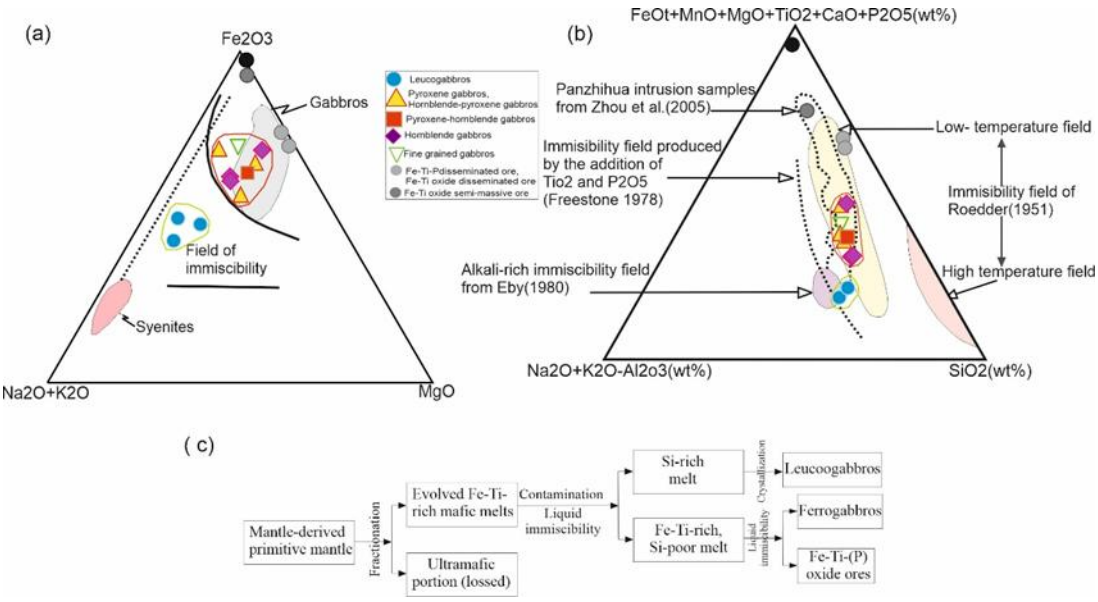

Fig. 17. a) Na_2O + K_2O–Fe_2O_3–MgO ternary digram (Philpotts, 1979). **b)** Pseudoternary Greig diagram showing fields of low- and high-temperature immiscibility in the system leucite-fayalite-SiO2 adapted from (Roedder, 1978). The three components are SiO_2, CaO + MgO + FeO(t) + TiO_2 + P_2O_5, and Na_2O + K_2O + Al_2O_3 plotted as wt%, showing the composition to (Roedder, 1951) Low and high temperature liquid immiscibility in the system K_2O–FeO–Al_2O_3–SiO_2, Panzhihua intrusion (Zhou et al., 2005), Akali-rich immisciblity (Eby, 1980) and immisciblity field produced by adation TiO_2–P_2O_5 (Freestone, 1978). **c)** simplified schematic model shows the evolution of mantle-derived magma and generation of Abu Murrat Fe-Ti-(P) oxide ores.

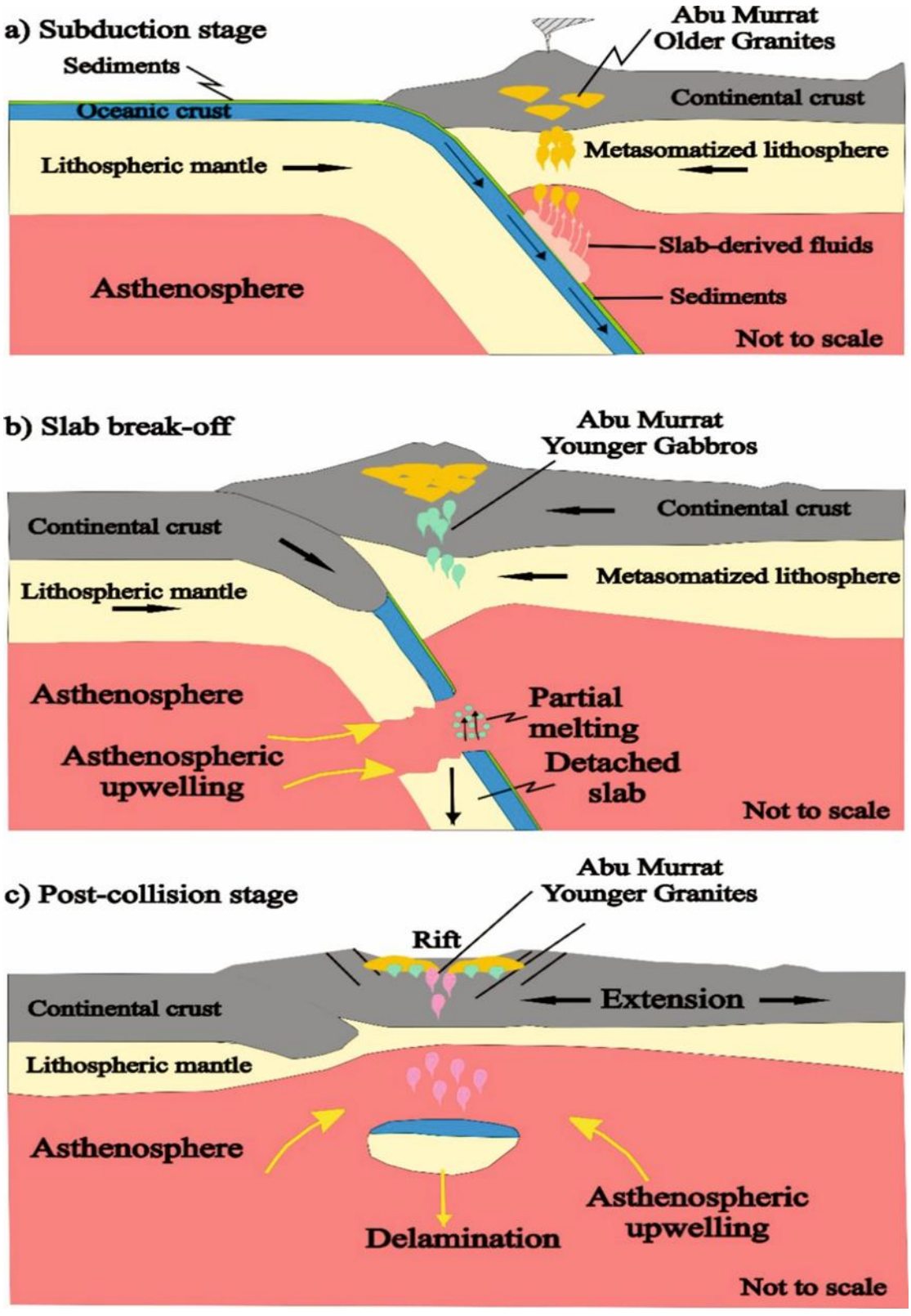

Fig. 18. Proposed schematic diagram show emplacement stages for Older Granites, Younger Gabbros, and Younger Granites.

The emplacement of the Abu Murrat A-type monzogranites followed a sequence of crustal thickening and lithospheric removal, attributed to slab break-off (Schott and Schmeling, 1998) (Fig. 18c). This process initiated significant asthenospheric upwelling (Avigad and Gvirtzman, 2009), which enriched the lithosphere in HFSE and alkalis (Fig. 13e) and facilitated partial melting. According to Martin (2006), such upwelling releases alkali- and silica-enriched fluids capable of metasomatizing both the mantle and crust. In the Abu Murrat case, these high-temperature mantle-derived melts induced partial melting of pre-existing tonalitic rocks within the lower crust, forming post-collisional, metaluminous to peraluminous magmas. As these magmas ascended, fractional crystallization further evolved their composition, producing the present-day monzogranites that intruded the Older Granites and Younger Gabbros (Fig. 18). This post-orogenic emplacement model aligns with earlier studies that associate A-type granite generation with extensional regimes during the collapse of the Pan-African Orogeny (Azer et al., 2019; Seddik et al., 2020; El-Awady et al., 2024).

Conclusion

1. The Abu Murrat complex represents a composite intrusion that records multiple magmatic episodes during transition from compressional to extensional tectonic settings in the evolution of the ANS. It comprises three major suites: (Older Granites, Younger Gabbros, Younger Granites).

2. The Abu Murrat Older Granites are mainly calc-alkaline, magnesian, and metaluminous, corresponding to I-type granitoids. In contrast, the Younger Granites display alkaline tendencies, range from metaluminous to peraluminous, vary from ferroan to magnesian, and share characteristics with A-type granitoids.

3. The Older Granites are richer in LILE (Rb, Ba, Sr) than in HFSE (Nb, Zr, Ti), a pattern consistent with arc-related magmatism akin to syn-tectonic I-type granites of the Eastern Desert, Egypt. Their evolution is interpreted to involve assimilation–fractional crystallization, where Mantle magmas mixed with crustal material during their ascent and emplacement.

4. The Younger Granites (A-type) show REE-normalized patterns with pronounced negative Eu anomalies, matching the geochemical traits of post-collisional A-type granites worldwide. These are inferred to have originated from partial melting of a juvenile, likely tonalitic, lower crustal source within a post-collisional tectonic regime.

5. Overall, the Abu Murrat granitoids record multiple magmatic stages during the development of the Arabian–Nubian Shield, beginning with Older Granite emplacement in a volcanic arc environment during subduction, and culminating in Younger Granite intrusion under post-collisional conditions, driven by lithospheric delamination and partial melting of a tonalitic crustal source.

6. The younger layered gabbros consist of pyroxene gabbros, hornblende-rich varieties, and leucogabbros, hosting Fe-Ti-(P) oxide ores. These rocks crystallized from highly evolved ferrobasaltic tholeiitic melts, likely derived from upwelling mantle plumes in a continental rift setting. They were subjected to extensive fractionation and crustal contamination and crystallized under high fO_2, temperatures of 800–1150 °C, and pressures of 2–5 kbar. Late-stage liquid immiscibility produced massive to disseminated Fe-Ti-(P) ores, comparable to Bushveld- and Skaergaard-type intrusions.

References

1. Abdelfadil, K. M., Saleh, G. M., Putiš, M., & Sami, M., 2022. Mantle source characteristics of the late Neoproterozoic post-collisional gabbroic intrusion of Wadi Abu Hadieda, north Arabian-Nubian Shield, Egypt. Journal of African Earth Sciences, 194, 104607.

2. Abdelfadil, K.M., Romer, R., Seifert, T., Lobst, R., 2013. Calc-alkaline lamprophyres from Lusatia (Germany) evidence for a repeatedly enriched mantle source. Chemical Geology,353, 230–245.

3. Abed, N. S., Monsif, M. A., Zakaly, H. M., & Awad, H. A., 2021. Geological and Mineralogical Investigations of Microgranites at the Southeastern Part of Wadi Baroud, North Eastern Desert, Egypt. Journal of Radiation and Nuclear Applications, 6, 135-149.

4. Abu Anbar, M.M., 2009. Petrogenesis of the Nesryin gabbroic intrusion in SW Sinai, Egypt: new contributions from mineralogy, geochemistry, Nd and Sr isotopes. Mineralogy and Petrology, 95, 87–103.

5. Abuamarah, B. A., Alzahrani, H., Matta, M. J., Azer, M. K., Asimow, P. D., & Darwish, M. H., 2023. Petrological, geochemical and geodynamic evolution of the Wadi Al-Baroud granitoids, north Arabian-Nubian shield, Egypt. Journal of African Earth Sciences, 207, 105044.

6. Adam, M.M.A., Lv, X., Fathy, D., Abdel Rahman, A.R.A., Ali, A.A., Mohammed, A.S., Farahat, E.S., Sami, M., 2022. Petrogenesis and tectonic implications of Tonian island arc volcanic rocks from the Gabgaba Terrane in the Arabian-Nubian Shield (NE Sudan). Journal of Asian Earth Sciences. 223, 105006.

7. Agrawal, S., Guevara, M., Verma, S.P., 2008. Tectonic discrimination of basic and ultrabasic volcanic rocks through log-transformed ratios of immobile trace elements. International Geology Review, 50(12), 1057–1079.

8. Akinin, V.V.; Miller, E.L.; Wooden, J.L., 2009. Petrology and geochronology of crustal xenoliths from the Bering Strait region: Linking deep and shallow processes in extending continental crust. In Crustal Cross Sections from the Western North American Cordillera and Elsewhere: Implications for Tectonic and Petrologic Processes: Geological Society of America Special Paper; Geological Society of America: Boulder, CO, USA, Volume 456, pp. 39–68.

9. Ali, K.A., Moghazi, A.M., Maurice, A.E., Omar, S.A., Wang, Q., Wilde, S.A., Moussa, E.M., Manton, W.I., Stern, R.J., 2012. Composition, age, and origin of the 620 Ma Humr Akarim and Humrat Mukbid A-Type granites: no evidence for preNeoproterozoic basement in the Eastern Desert, Egypt. International Journal of Earth Sciences, 101, 1705–1722.

10. Ali, K.A., Wilde, S.A., Stern, R.J., Moghazi, A.-K.M., Ameen, S.M.M., 2013. Hf isotopic composition of single zircons from Neoproterozoic arc volcanics and postcollision granites, Eastern Desert of Egypt: implications for crustal growth and recycling in the Arabian-Nubian Shield. Precambrian Research, 239, 42–55.

11. Ali, S., Ntaflos, T., Sami, M., 2021. Geochemistry of Khor Um-Safi ophiolitic serpentinites, central Eastern desert, Egypt: implications for neoproterozoic arcbasin system in the Arabian-Nubian shield. Geochemistry 81, 125690.

12. Anderson, J. L., Smith, D. R., 1995. The effects of temperature and fO2 on the Al-in-hornblende barometer. American Mineralogist, 80(5-6), 549–559.

13. Attawiya, M., Nossair, L., El-Debeiky, A., Ragab, A., 1996. Geology, Petrography, Geochemistry, and Geochronology of the Old Granite Batholith between Quen and Safaga, Eastern Desert, Egypt. Proceedings of the 6th Conference of Nuclear Sciences and Applications, Cairo, Egypt.

14. Avigad, D., Gvirtzman, Z., 2009. Late Neoproterozoic rise and fall of the northern Arabian-Nubian shield: the role of lithospheric mantle delamination and subsequent thermal subsidence. Tectonophysics, 477, 217–228.

15. Awad, H. A., El-Leil, I. A., El-Wardany, R. M., Ene, A., Tolba, A., Kamel, M., & Zakaly, H. M., 2022a. Mineralogy and radioactivity level of the new occurrence of ilmenite bearing gabbro at Abu Murrat, Northeastern Desert, Egypt. Romanian Journal of Physics, 67, 803.

16. Awad, H. A., El-Leil, I. A., Kamel, M., Tolba, A., Nastavkin, A. V., & El-Wardany, R. M., 2022b. Geological features identified from field observations and remote sensing data on the Um Taghir area, Eastern Desert, Egypt. Geodinamika i tektonofizika, 13(3), 14.

17. Azer, M.K., Gahlan, H.A., Asimow, P.D., Mubarak, H.S., Al-Kahtany, K.M., 2019. Multiple stages of carbonation and element redistribution during formation of ultramafic-hosted magnesite in Neoproterozoic ophiolites of the Arabian-Nubian Shield, Egypt. Journal of Geology, 127 (1), 81–107.

18. Batchelor, R.A., Bowden, P., 1985. Petrogenetic interpretation of granitoid rock series using multicationic parameters. Chemical Geology, 48, 43–55.

19. Be'eri-Shlevin, Y., Eyal, M., Eyal, Y., Whitehouse, M.J., Litvinovsky, B., 2012. The Sa'al volcano-sedimentary complex (Sinai, Egypt): a latest Mesoproterozoic volcanic arc in the northern Arabian Nubian Shield. Geology, 40, 403–406.

20. Bonin, B., 2007. A-type granites and related rocks: evolution of a concept, problems and prospects. Lithos, 97, 1–29.

21. Buddington, A.F., Lindsley, D.H., 1964. Iron-Titanium Oxide Minerals and Synthetic Equivalents. Journal of Petrology, 5(2), 310–357.

22. Černý P., 1989. Characteristics of pegmatite deposits of tantalum. In: Möller P (ed) Lanthanides, tantalum, and niobium. Springer, Berlin, pp 195–239

23. Chappell, B. W., & Wyborn, D. ,2012. Origin of enclaves in S-type granites of the Lachlan Fold Belt. Lithos, *154*, 235-247.

24. Chen, B., & Jahn, B. M.,2002. Geochemical and isotopic studies of the sedimentary and granitic rocks of the Altai orogen of northwest China and their tectonic implications. Geological Magazine, 139(1), 1-13.

25. Cox, K. G. (Ed.)., 2013. The interpretation of igneous rocks. Springer Science & Business Media

26. De la Roche, H., Leterrier, J., Grand Claude, P., Marchal, M., 1980. A classification of volcanic and plutonic rocks using R1–R2 diagrams and major element analyses – its relationships and current nomenclature. Chemical Geology, 29, 183–210

27. Desta, M. T., Ayalew, D., Ishiwatari, A., Arai, S., Tamura, A., 2014. Ferropicrite from the Lalibela area in the Ethiopian large igneous province. Journal of Mineralogical and Petrological Sciences, 109(4), 191–207.

28. El Mahallawi, M.M., Ahmed, A.F., 2012. Late Proterozoic older granitoids from theNorth Eastern desert of Egypt: petrogenesis and geodynamic implications. Arabian Journal of Geosciences,5, 15–27.

29. El-Awady, A., Abdelnaiem, D. A., Kharbish, S., Awad, H. A., Kumral, M., Kaya, M., & Abdelnasser, A., 2025. Petrogenesis of Fe-Ti-(P) oxide bearing layered gabbroic intrusion in the Northern Eastern Desert of Egypt: insights into parent melt composition and genesis of oxide ores. Journal of African Earth Sciences, 105780.

30. El-Awady, A., Sami, M., Abart, R., Fathy, D., Farahat, E. S., Ahmed, M. S., ... & Ragab, A., 2024. Petrogenesis and Tectonic Evolution of I-and A-Type Granites of Mount Abu Kibash and Tulayah, Egypt: Evidence for Transition from Subduction to Post-Collision Magmatism. Minerals, 14(8), 806.

31. El-Bialy, M. Z., & Omar, M. M., 2015. Spatial association of Neoproterozoic continental arc I-type and post-collision A-type granitoids in the Arabian–Nubian Shield: the Wadi Al-Baroud older and younger granites, north eastern desert, Egypt. Journal of African Earth Sciences, 103, 1-29.

32. Eldougdoug, A., Abd El-Rahman, Y., Harbi, H., 2020. The Ediacaran post-collisional Khamal gabbro-anorthosite complex from the Arabian Shield and its Fe-Ti-P ore: an analogy to Proterozoic massif-type anorthosites. Lithos, 372, 105674.

33. El-Gaby, S., List, F. K., & Tehrani, R., 1988. Geology, evolution and metallogenesis of the Pan-African belt in Egypt. In The Pan-African belt of Northeast Africa and adjacent areas: tectonic evolution and economic aspects of a late proterozoic Oregon (pp. 17-68). Springer. https://doi.org/10.1007/978-3-642-73069-5_2

34. El-Nisr, S.A., El-Sayed, M.M., Saleh, 1388 G.M., 2001. Geochemistry and petrogenesis of Pan-African late- to post-orogenic younger granitoids at Shalatin-Halaib, south Eeastern Desert, Egypt. Journal of African Earth Sciences 33, 261–282.

35. Eyal, M., Litvinovsky, B., Jahn, B.M., Zanvilevich, A., Katzir, Y., 2010. Origin and evolution of post-collisional magmatism: coeval Neoproterozoic calcalkaline and alkaline suites of the Sinai Peninsula. Chemical Geology, 269, 153–179.

36. Fleet, M.E, Barnett, R.L., 1978. Aliv/Alvi partitioning in calciferous amphiboles from the Frood mine, Sudbury, Ontario. The Canadian Mineralogist, 16, 527–532.

37. Frihy, O. E., 2007. The Nile Delta: processes of heavy mineral sorting and depositional patterns. Developments in Sedimentology, 58, 49-74.

38. Fritz, H., Abdelsalam, M., Ali, K.A., Bingen, B., Collins, A.S., Fowler, A.R., Ghebreab, W., Hauzenberger, C.A., Johnson, P.R., Kusky, T.M., Macey, P., Muhongo, S., Stern, R.J., Viola, G., 2013. Orogen styles in the East African Orogen: a review of the Neoproterozoic to Cambrian tectonic evolution. Journal of African Earth Sciences, 86, 65–106.

39. Frost, B.R., Barnes, C.G., Collins, W.J., Arculus, R.J., Ellis, D.J., Frost, C.D., 2001. A geochemical classification for granitic rocks. Journal of Petrology, 42 (11), 2033–2048.

40. Frost, C.D., Frost, B.R., 2011. On Ferroan (A-type) Granitoids: their Compositional Variability and Modes of Origin. Journal of Petrology, 52, 39-53.

41. Gibson, S. A., Thompson, R. N., Dickin, A. P., 2000. Ferropicrites: geochemical evidence for Fe-rich streaks in upwelling mantle plumes. Earth Planet. Sci. Lett. 174(3–4), 355–374.

42. Greiling, R.O., Abdeen, M.M., Dardir, A.A., El Akhal, H., El Ramly, M.F., Kamal El Din, G.M., Osman, A.F., Rashwan, A.A., Rice, A.H.N., Sadek, M.F., 1994. A structural synthesis of the Proterozoic Arabian-Nubian Shield in Egypt. Geologische Rundschau, 83, 484–501.

43. Hamimi, Z., Fowler, A.-R., Liegeois, J.-P., Collins, A., Abdelsalam, M., Abd El-Wahed, M. (Eds.), 2021. The Geology of the Arabian-Nubian Shield, Regional Geology Reviews Book Series (RGR), vol. 786p. Springer Nature Switzerland. https://10.1007/978-3 -030-72995-0.

44. Hargrove, U.S., Stern, R.J., Kimura, J.-I., Manton, W.I., Johnson, P.R., 2006. How juvenile is the Arabian-Nubian Shield? Evidence from Nd isotopes and pre Neoproterozoic inherited zircon in the Bi'r Umq suture zone, Saudi Arabia. Earth and Planetary Science Letters, 252, 308–326

45. Hassan, M.A., Hashad, A.H., 1990. Precambrian of Egypt. In: Said, R. (Ed.), The Geology of Egypt. Alkema, Rotterdam, pp. 201–245.

46. Hayashi, K. I., Fujisawa, H., Holland, H. and Ohmoto, H., 1997. Geochemistry of ~1.9 Ga sedimentary rocks from northeastern Labrador, Canada, Geochimica et Cosmochimica Acta, 61(19), 4115-4137

47. He, H. L., Yu, S. Y., Song, X. Y., Du, Z. S., Dai, Z. H., Zhou, T., Xie, W., 2016. Origin of nelsonite and Fe–Ti oxides ore of the Damiao anorthosite complex, NE China: Evidence from trace element geochemistry of apatite, plagioclase, magnetite and ilmenite. Ore Geology Reviews, 79, 367–381.

48. Hussein, A.A., Aly, M.M., El Ramly, M.F., 1982. A proposed new classification of the granites of Egypt. Journal of Volcanology and Geothermal Research, 14, 187–198.

49. Irvine, T. N., & Baragar, W. R. A. F., 1971. A guide to the chemical classification of the common volcanic rocks. Canadian journal of earth sciences, 8(5), 523-548.

50. Johnson, P.R., Andresen, A., Collins, A.S., Fowler, A.R., Fritz, H., Ghebreab, W., Kusky, T., Stern, R.J., 2011. Late Cryogenian-Ediacaran history of the Arabian-Nubian Shield: a review of depositional, plutonic, structural, and tectonic events in the closing stages of the northern East African Orogen. Journal of African Earth Sciences, 61, 167–232.

51. Khalil, A., Obeid, M., Azer, M., 2015. Late Neoproterozoic post-collisional mafic magmatism in the Arabian–Nubian Shield: a case study from Wadi El-Mahash gabbroic intrusion in southeast Sinai, Egypt. Journal of African Earth Sciences , 105, 29–46.

52. Khalil, K., Summers, P., El-Shazly, A., 2023. Origin of the post-collisional younger gabbroic rocks and the associated Fe–Ti oxide ores, Abu Ghalaga area, Southern Eastern Desert, Egypt: mineralogical and geochemical constraints. Arabian Journal of Geosciences, 16(3), 160.

53. Khedr, M. Z., El-Awady, A., Arai, S., Hauzenberger, C., Tamura, A., Stern, R. J., Morishita, T., 2020. Petrogenesis of the ~740 Korab Kansi mafic-ultramafic intrusion, South Eastern Desert of Egypt: Evidence of Ti-rich ferropicritic magmatism. Gondwana Research, 82, 48–72.

54. Khedr, M. Z., Moftah, A., El-Shibiny, N. H., Tamura, A., Tan, W., Ichiyama, Y., ... & Abdelrahman, K., 2024. Mineralogy and Geochemistry of Titaniferous Iron Ores in El-Baroud Layered Gabbros: Fe-Ti Ore Genesis and Tectono-Metallogenetic Setting. Minerals, 14(7), 679.

55. Khedr, M. Z., Takazawa, E., Arai, S., Stern, R. J., Morishita, T., and El-Awady, A. 2022, Styles of Fe–Ti–V ore deposits in the Neoproterozoic layered mafic-ultramafic intrusions, south Eastern Desert of Egypt: Evidence for fractional crystallization of V-rich melts. Journal of African Earth Sciences, 194, 104620.

56. Kroner, A., Kruger, J., Rashwan, A.A., 1994. Age and tectonic setting of granitoid gneisses in the Eastern Desert of Egypt and south–west Sinai. Geologische Rundschau, 83, 502–513.

57. Leterrier, J., Maury, R. C., Thonon, P., Girard, D., Marchal, M., 1982. Clinopyroxene composition as a method of identification of the magmatic affinities of paleo-volcanic series. Earth Planet. Science letters journal, 59(1), 139–154.

58. Luan, Y., Song, X. Y., Chen, L. M., Zheng, W. Q., Zhang, X. Q., Yu, S. Y., She, Y. W., Tian, X. L., Ran, Q. Y., 2014. Key factors controlling the accumulation of the Fe–Ti oxides in the Hongge layered intrusion in the Emeishan Large Igneous Province, SW China. Ore Geology Reviews, 57, 518–538.

59. Lustrino, M., 2006. Composition, petrography, and mineral chemistry of ODP Site 1224 Eocene ferrobasalts (Leg 200; North Pacific Ocean). In Proceedings of the Ocean Drilling Program 200, 1–25.

60. Maniar, p. d. & Piccoli, p. M., 1989: Tectonic discrimination of granitoids. Geological Society of America Bulletin, 101: 635–643.

61. Mansouri-Esfahani M, Khalili M, Kochhar N and Gupta LN, 2010. A-type granite of the Hasan-Robat area (NW of Isfahan, Iran) and its tectonic significance. Journal of Asian Earth Sciences 37(3): 207–218, DOI 10.1016/j.jseaes.2009.05.010.

62. McDonough, W.F., Sun, S., 1995. The composition of the Earth. Chemical Geology, 120, 223–253.

63. McDonough, W.F., Sun, S., 1995. The composition of the Earth. Chemical Geology, 120, 223–253.

64. Middlemost, E.A.K., 1994. Naming materials in the magma/igneous rock system. Earth-Science Reviews, 37, 215–224.

65. Moghazi, A.M., 2002. Petrology and geochemistry of Pan-African granitoids, Kab Amiri area, Egypt—implications for tectonomagmatic stages of the Nubian Shield evolution. Mineralogy and Petrology, 75, 41–67.

66. Moussa, E.M.M., Stern, R.J., Manton, W.I., Ali, K.A., 2008. SHRIMP zircon dating and Sm/Nd isotopic investigations of Neoproterozoic granitoids, Eastern Desert, Egypt. Precambrian Research, 160, 341–356.

67. Namur, O., Charlier, B., and Holness, M. B., 2012, Dual origin of Fe–Ti–P gabbros by immiscibility and fractional crystallization of evolved tholeiitic basalts in the Sept Iles layered intrusion. Lithos, 154, 100-114.

68. Namur, O., Charlier, B., Toplis, M.J., Higgins, M.D., Liégeois, J.-P., VanderAuwera, J., 2010. Crystallization sequence and magma chamber processes in the Ferrobasaltic sept Iles layered intrusion, Canada. J. Petrol. 51, 1203–1236

69. Omran, A., 2014 .Geology, mineralogy and radioelements potentiality of microgranite dikes to the south of Abu Hadieda area, Northern Eastern Desert, Egypt. A l-Azhar Bulletin of Science, 25, 47–62. [CrossRef]

70. Patino Douce, A.E., 1999. What do experiments tell us about the relative contributions of crust and mantle to the origin of granitic magmas. In: Castro, A., Fernández, C., Vigneresse, J.L. Eds., Understanding Granites: Integrating New and Classical Techniques. Geological Society of London Special Publication 168, pp. 55–75.

71. Pearce, J. A., Harris, N. B., & Tindle, A. G., 1984. Trace element discrimination diagrams for the tectonic interpretation of granitic rocks. Journal of petrology, 25(4), 956-983.

72. Prowatke, S.; Klemme, S., 2006. Trace element partitioning between apatite and silicate melts. Geochimica et Cosmochimica Acta, 70, 4513–4527. [CrossRef]

73. Robinson, F. A., Foden, J. D., Collins, A. S., Payne, J. L., 2014. Arabian Shield magmatic cycles and their relationship with Gondwana assembly: insights from zircon U–Pb and Hf isotopes. Earth and Planetary Science Letters , 408, 207–225.

74. Rollison, H.R.,1993. Using Geochemical Data: Evaluation, Presentation, Interpretation; Longman: Singapore, 1993; p. 352.

75. Samuel, M., Ghabrial, D., Moussa, H., Ali-Bik, M., 2015. The petrogenesis of late Neoproterozoic gabbro/diorite intrusion at Sheikh El-Arab area, central Sinai, Egypt. Arabian Journal of Geosciences, 8, 5579–5599.

76. Schott, B., & Schmeling, H., 1998. Delamination and detachment of a lithospheric root. Tectonophysics, 296(3-4), 225-247.

77. Seddik, A.M.A.; Darwish, M.H.; Azer, M.K.; Asimow, P.D., 2020. Assessment of magmatic versus post-magmatic processes in the Mueilha rare-metal granite, Eastern Desert of Egypt, Arabian-Nubian Shield. Lithos, 366, 105542. [Google Scholar] [CrossRef].

78. Soesoo, A., 1997. A multivariate statistical analysis of clinopyroxene composition: Empirical coordinates for the crystallisation PT-estimations. GFF, 119(1), 55–60.

79. Song, X.Y.; Qi, H.W.; Hu, R.Z.; Chen, L.M.; Yu, S.Y.; Zhang, J.F., 2013. Formation of thick stratiform Fe-Ti oxide layers in layered intrusion and frequent replenishment of fractionated mafic magma: Evidence from the Panzhihua intrusion, SW China. Geochemistry, Geophysics, Geosystems, 2013, 14, 712–732.

80. Stern, R.J., 1979. Late Precambrian Ensimatic Volcanism in the Central Eastern Desert of Egypt. Ph.D. Thesis, California University, San Diego, 210 pp.

81. Stern, R.J., 1994. Arc assembly and continental collision in the Neoproterozoic East African Orogen: implications for the consolidation of Gondwanaland. Annual Review of Earth and Planetary Sciences, 22, 319–351.

82. Stern, R.J., 2002. Crustal evolution in the East African Orogen: a neodymium isotopic perspective. Journal of African Earth Sciences, 34, 109–117.

83. Stern, R.J., 2008. Neoproterozoic crustal growth: the solid Earth system during a critical episode of the Earth history. Gondwana Research, 14, 33–50.

84. Stern, R.J., Hedge, C.E., 1985. Geochronologic and isotopic constraints on Late Precambrian crustal evolution in the Eastern Desert of Egypt. American journal of science, 285, 97–127.

85. Stern, R.J., Johnson, P.R., 2010. Continental lithosphere of the Arabian Plate. A geologic, petrologic, and geophysical synthesis. Earth-Science Reviews, 101, 29–67.

86. Sun, S. S., and McDonough, W. S., 1989, Chemical and isotopic systematics of oceanic basalts: Implications for mantle composition and processes. Geological Society of London, Special Publications, 42(1), 313–345.

87. Tuff, J., Takahashi, E., Gibson, S. A., 2005. Experimental constraints on the role of garnet pyroxenite in the genesis of high-Fe mantle plume derived melts. Journal of Petrology, 46(10), 2023–2058.

88. Vaughan, A.P.M., Pankhurst, R.J., 2008. Tectonic overview of the West Gondwana margin. Gondwana Research, 13, 150–162.

89. Whalen, J.B., Currie, K.I., Chappell, B.W., 1987. A-type granites: geochemical characteristic, discrimination and petrogenesis. Contributions to Mineralogy and Petrology, 95, 407–419.

90. Zhou, M.F.; Robinson, P.T.; Lesher, C.M.; Keays, R.R.; Zhang, C.J., 2005. Malpas, J. Geochemistry, Petrogenesis and Metallogenesis of the Panzhihua Gabbroic Layered Intrusion and Associated Fe–Ti–V Oxide Deposits, Sichuan Province, SW China. Journal of Petrology, 46, 2253–2280. [CrossRef]

91. Sami, M., Osman, H., Ahmed, A. F., Zaky, K. S., Abart, R., Sanislav, I. V., ... & Abbas, H., 2023. Magmatic evolution and rare metal mineralization in Mount El-Sibai peralkaline granites, central Eastern Desert, Egypt: Insights from whole-rock geochemistry and mineral chemistry data. Minerals, 13(8), 1039.

92. Sami, M.; El Monsef, M.A.; Abart, R.; Toksoy-Köksal, F.; Abdelfadil, K.M.,2022. Unraveling the Genesis of Highly Fractionated Rare-Metal Granites in the Nubian Shield via the Rare-Earth Elements Tetrad Effect, Sr–Nd Isotope Systematics, and Mineral Chemistry. ACS Earth and Space Chemistry, 6, 2368–2384.

93. Sami, M.; Adam, M.M.; Lv, X.; Lasheen, E.S.R.; Ene, A.; Zakaly, H.M.; Alarifi, S.S.; Mahdy, N.M.; Abdel Rahman, A.R.A.; Saeed, A.,2023. Petrogenesis and Tectonic Implications of the Cryogenian I-Type Granodiorites from Gabgaba Terrane (NE Sudan). Minerals, 13, 331.